OPTICAL PROBE DESIGN FOR CONTINUOUS WAVE NEAR-INFRARED SPECTROSCOPY

by

Kadir Evcil

B.Sc., in Electronics Engineering, Istanbul University, 2005

Submitted to the Institute of Biomedical Engineering
in partial fulfillment of the requirements
for the degree of
Master of Science
in
Biomedical Engineering

Boğaziçi University
January 2009

ACKNOWLEDGMENTS

First, I would like to thank my advisor Assoc. Prof. Ata AKIN for his support and leadership during my thesis. He has patiently guided me through my thesis and encouraged my studies.

I would also like to thank to Assoc. Prof. Dr. H. Özcan GÜLÇÜR and Assistant Prof. Kıvanç MIHÇAK for their support.

I would also like to thank to my friends Ömer Şaylı, Turan Deniz Nevşehirli, Murat Tümer and Gökçen Yıldız for sharing their knowledge and experience.

I would also like to thank to all of my test subjects.

Last, I would like to thank my family, especially to my mother who continuously supported me and encouraged my studies.

ABSTRACT

OPTICAL PROBE DESIGN FOR CONTINUOUS WAVE NEAR-INFRARED SPECTROSCOPY

The modern medicine is using optical methods more and more every day, among optical methods Near-infrared Spectroscopy is one of the most appealing techniques. Near-infrared spectroscopy is a noninvasive, safe, reliable technique. With near-infrared spectroscopy even three dimensional images can be produced and functional information can be achieved. Near infrared spectroscopy uses light at the infrared portion of the electromagnetic spectrum and measures the changes in the intensity of the light.

This M.S. thesis is focused on the development of a prototype Near Infrared Spectroscopy instrument. This instrument is based on the Continuous Wave Near-Infrared Spectroscopy. This system is designed by using leds that emit near-infrared light, photodiode detectors that are sensitive to near-infrared light, and operational amplifiers. The instrument's circuit design is based on the analog circuit design. The ability and effectiveness of the system is tested on phantom and human subjects with several experiments.

Keywords: Functional, Near, Infrared, Spectroscopy, Continuous Wave, Muscle, Optical, Imaging.

ÖZET

DEVAMLI DALGA YAKIN KIZILALTI SPEKTROSKOPİ İÇİN OPTİK PROB DİZAYNI

Modern tıp optik metotları günden güne daha çok kullanıyor, optik metotların içinde Yakın Kızılaltı Spektroskopi en çekici tekniklerden biridir. Yakın Kızılaltı Spektroskopi noninvazif, güvenli, güvenilir bir tekniktir. Yakın Kızılaltı Spektroskopi ile üç boyutlu görüntüler üretilebilir ve fonksiyonel bilgiye ulaşılabilir. Yakın Kızılaltı Spektroskopi elektromanyetik spektrumun kızılaltı bölgesindeki ışığı kullanır ve ışığın yoğunluğundaki değişimleri ölçer.

Bu yüksek lisans tezi bir prototip Yakın Kızılaltı Spektroskopi cihazı geliştirilmesi üzerine odaklanmıştır. Cihaz, Devamlı Dalga Yakın Kızılaltı Spektroskopi metodunu üzerine temellendirilmiştir. Bu sistem yakın kızılaltı ışık yayan diyotlar, yakın kızılaltı ışığa duyarlı detektörler ve kuvvetlendiricilerle yapılmıştır. Bu cihazın devre dizaynı analog devre dizaynı üzerine temellendirilmiştir. Sistemin yetenekleri ve efektifliği fantom ve insan denekler üzerinde çeşitli deneylerle test edilmiştir.

Anahtar Sözcükler: Fonksiyonel, Yakın, Kızılaltı, Spektroskopi, Devamlı Dalga, Kas, Optik, Görüntüleme.

TABLE OF CONTENTS

LIST OF FIGURES

LIST OF TABLES

LIST OF SYMBOLS

A	Attenuation measured in optical densities
c	The concentration of the absorbing compound
d	Optical path-length
I_o	The light intensity incident on the medium
a	Specific extinction coefficient
μ_a	absorption coefficient
N	The number density of the scattering particles
s	The scattering cross section of the particles
DP	The differential (true) path-length
DPF	Scaling factor of differential (true) path-length
R	Resistor
C	Capacitor
f	Frequency
V	Voltage
A	Ampere
L	Length
W	Width
H	Heigth
dc	Direct current
ac	Alternating current
I_{dc}	dc current
I_{ac}	ac current
V_{offset}	dc voltage - offset voltage

LIST OF ABBREVIATIONS

NIRS	Near-infrared spectroscopy
fNIRS	Functional near-infrared spectroscopy
PbS	Lead sulphide
oxy-Hb or HbO2	Oxygenated haemoglobin
deoxy-Hb or Hb	Deoxygenated haemoglobin
PAD	Peripheral arterial disease
ATP	Adenosine triphosphate
CtOx	Oxidized cytochrome oxidase
DPF	Differential Path-length Factor
CW	Continuous Wave
TRS	Time Resolved Spectroscopy
PMS	Phase Modulation Spectroscopy
SRS	Spatially Resolved Spectroscopy
DWS	Diffusing-wave spectroscopy
NIRI	Near Infrared Imaging
DOI	Diffuse optical imaging

1. INTRODUCTION

Near-Infrared Spectroscopy (NIRS) is a technique that measures the concentration changes in the blood oxygenation of brain, muscles, and breasts. NIRS posses virtually no harm to humans, it does not use any harmful radiation or does not use radioactive agents like positron emission tomography or x-ray. When using NIRS, patients can be examined repeatedly or continuously with NIRS system [5].

NIRS is a low cost, compact, portable, low power technique with high temporal resolution. NIRS penetrates the skin and fat, and due high absorption of chromophores the change in the concentration of blood deoy-Haemoglobin and oxy-Haemoglobin can be measured.

Measurements are analyzed by using Modified Beer Lambert Law. Modified Beer Lambert Law states that the attenuation of an absorbing compound dissolved in a non-scattering solvent is directly proportional to the product of the concentration of the compound and the optical path-length [12].

The objective of my M.Sc. thesis is to make contribution to the development of a continuous wave near-infrared spectroscopy instrument at Boğaziçi University to enable muscle studies to be done at faster speeds.

1.1 Outline

In this thesis I tried to provide a background of the NIRS from historic, clinical, and technological aspects. Most of this thesis is involved with design and results from the instrument.

Chapter 2 contains history, development, and an introduction to muscle physi-

ology of the human skeletal muscles.

Chapter 3 introduces the physical and mathematical background of near-infrared light through tissues, and summaries the current and past NIRS systems both commercial and experimental.

Chapter 4 involves the system design and results taken from experiments on phantoms.

Chapter 5 has the discussion of the work so far done.

2. FUNCTIONAL NEAR-INFRARED SPECTROSCOPY

Near-infrared spectroscopy is a technique used in biomedical science for monitoring blood oxygenation in brain, breast and muscle [13, 14, 15, 8]. NIRS is a non-invasive, reliable, safe technique that uses light in the near-infrared spectrum (between 650-950 nm) of the electromagnetic spectrum [13, 11, 16, 17, 14, 15, 8]. NIRS provides high temporal resolution, relatively low spatial resolution, and is inexpensive and portable [8].

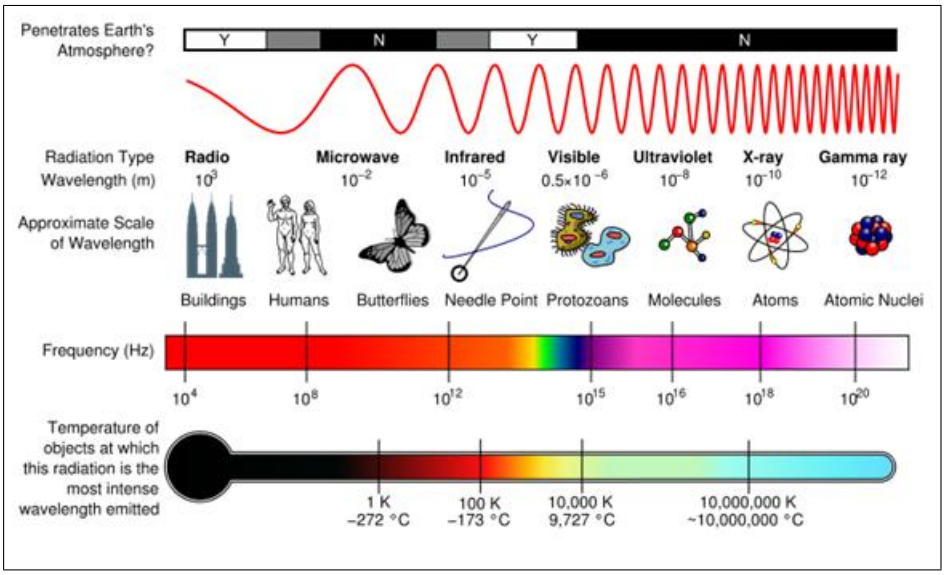

Figure 2.1 Electromagnetic Spectrum [1].

It basically consists of a probe with a light source and a detector, main unit for control purposes, and a computer [5]. Near-infrared light occupies the 700 nm-900 nm portion of the electromagnetic spectrum [13, 11, 16, 17, 14, 15].

2.1 History

Near-infrared spectroscopy's foundations date backs to A.D. 130, however most significant progress is done by Sir William Herschel. Sir William Herschel discovered the near-infrared radiation (19th century) [18]. During the 19th century evolution of

NIR devices continued steadily.

2.1.1 Development of NIR

W. W. Coblentz constructed a spectrometer using a rock-salt prism and a sensitive thermopile connected to a mirror galvanometer. He allowed the chemists to obtain structural information about compounds via spectroscopy [18].

At 1930s during World War 2 a new area was found that speed up the development of NIR. The idea is to use NIR as heat sensing device to be used in the war. 1930s. Kubelka and Munk's worked on the diffuse scattering of light in both transmission and reflection and so NIR measurement on solid started. It used lead sulphide (PbS) as the compound semiconductor, and made a very sensitive detector for the $1 to 2.5 \mu m$ wavelength region [18].

The use of semiconductor technology, especially the microprocessors and personal computers, increased the area of use and the speed of development of NIR devices due to the ability to control and acquire data from the instrument, and more to be able to facilitate calibration and data analysis [18].

2.1.2 Modern Era

The first biomedical application of the near infrared spectroscopy is made by Jöbsis (1977) by continuously monitoring physiological changes of a cat's head [11, 14, 15, 12, 19]. Ozaki et al. studied the venal blood to determine the level of deoxy-Hb [18].

Michael Sowa used NIR imaging to monitor regional and temporal variations in tissue oxygenation. Mancini et al. estimated skeletal muscle-oxygenation by using the differential absorption properties of the haemoglobin [18].

Lin et al. in 1998 studied the influence of fat layers on measuring the oxygenation of blood. Franceschini et al. in 1996 studied the effects of water on haemoglobin concentration in a tissue-like phantom [18]. Keiko Miyasaka used a device named Niroscope for NIR spectroscopy and found that Beer's law was not followed accurately if the signal was passed through the cranium [18].

Cooper et al. in 1998 studied on the adult brain with NIR and determined the effects of changes in the rate of oxygen delivery on adult rat-brain chemistry. Wyatt et al. used NIR to quantify the cerebral blood volume in human infants [18]. Mansfield et al. studied ischemia in the forearm in 1997. Hirth et al. studied the clinical application of NIR in Migraine patients [18].

Center for Biomedical Technology in Australia developed a device to measure oxygen content. It consisted of five 1W lasers at wavelengths of 780, 800, 830, 850, and 980 nm and used a photodiode receiver. It used the Hb/deoxy-Hb absorbance differences [18].

Hitachi used NIR to detect blood flow changes in the brain to determine sites of epileptic activity. The technique was able to determine the side of the brain where the episode was taking place in all the patients on which it was tried [18].

2.2 Functional Near Infrared Spectroscopy

Functional near-infrared spectroscopy (fNIRS) is a non-invasive method for monitoring blood oxygenation. Oxygen is carried with haemoglobin molecule in the blood. fNIRS monitors the changes in the oxygenated haemoglobin (oxy-Hb) and de-oxygenated haemoglobin (deoxy-Hb) concentration [13, 11, 16, 17, 14, 15, 8, 12].

fNIRS can monitor the oxy-Hb and deoxy-Hb level by using a optical window in near-infrared region (700nm-900nm) of the electromagnetic spectrum. In the NIR region the oxy-Hb and deoxy-Hb molecules have different optical characteristics.

At different wavelengths they both have high absorption rates in the NIR region of electromagnetic spectrum, whereas water and lipid has low absorption rates at those wavelengths [13, 11, 16, 17, 14, 15, 8, 12].

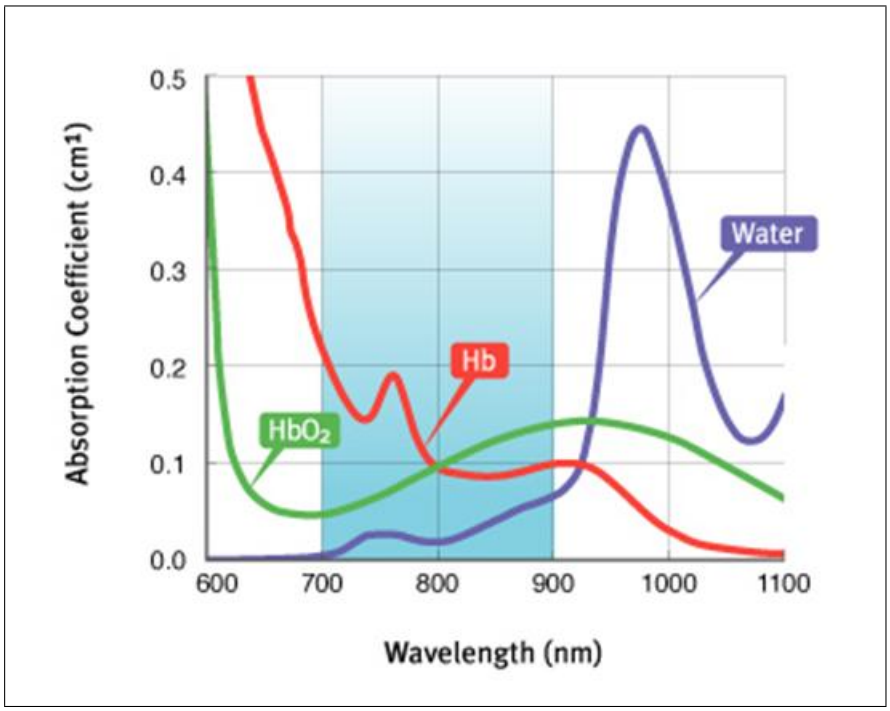

Figure 2.2 Absorption rates of Oxy-Hb, Deox-Hb and water in the near-infrared spectrum [2].

Physiological changes effects the functional state of the tissue which affects the optical properties of the blood. By monitoring blood oxygenation, the physiological changes in the human tissues can be observed.

2.3 Muscle Contraction

Noninvasive characterization of oxygen consumption and metabolism in skeletal muscles has important applications in exercise medicine and for understanding of vascular conditions such as peripheral arterial disease (PAD) [8].

Near-infrared spectroscopy is sensitive to smaller vessels such as arterioles, capillaries, and venules. In principle it can provide dynamic information about oxy- and

deoxy-hemoglobin concentrations, total hemoglobin concentration, and tissue blood oxygen saturation in deep muscle tissues [8].

Muscle is the organ that produces force. With the force generated, muscle allows locomotion of humans and animals; it allows us carry loads or lift things of various weighs. To do all these muscles require energy (ATP). Muscles' energy need in exercise, in example while running or lifting a dumbbell 50 times, requires a lot of ATP. To generate enough energy, oxygen is used in oxidative respiration to produce ATP.

The need to oxygen created from the exercise increases oxygen consumption, blood supplies more oxygen to the muscle. This physiological change can be monitored with functional near infrared spectroscopy to understand what happens during exercises, during muscles' working better NIRS is used investigate the skeletal muscle oxygenation and functioning of it.

2.3.1 Muscle Structure of Skeletal Muscles

The entire muscle is typically surrounded by a fascia and epimysium. Epimysium is a connective tissue. Muscle is made up of fascicles. Fascicle is a muscle bundle that consists of a number of muscle fibers and each fascicle is surrounded by perimysium. Perimysium is also a connective tissue.

Muscle fiber is an individual muscle cell. The muscle fibers are within a cell membrane called the sarcolemma and each muscle fiber is surrounded by the endomysium. Endomysium is a connective tissue. Muscle fibers are made up of myofibrils that lye parallel to one another. Muscle fibers are made up of sarcomeres. The sarcomere is the basic contractile unit of a muscle. Sarcomeres are comprised of actin and myosin myofilaments.

Sarcomeres are the basic force producing units of muscle and they are bordered

by the Z-discs. Myosin is located in the center of a sarcomere and the actin is bisected by Z-disks. The dark areas of the striation pattern in skeletal muscle are myosin filaments because of that they are called A-bands. The light pattern of the skeletal muscle is made up by actin filaments because of that they are called I-bands.

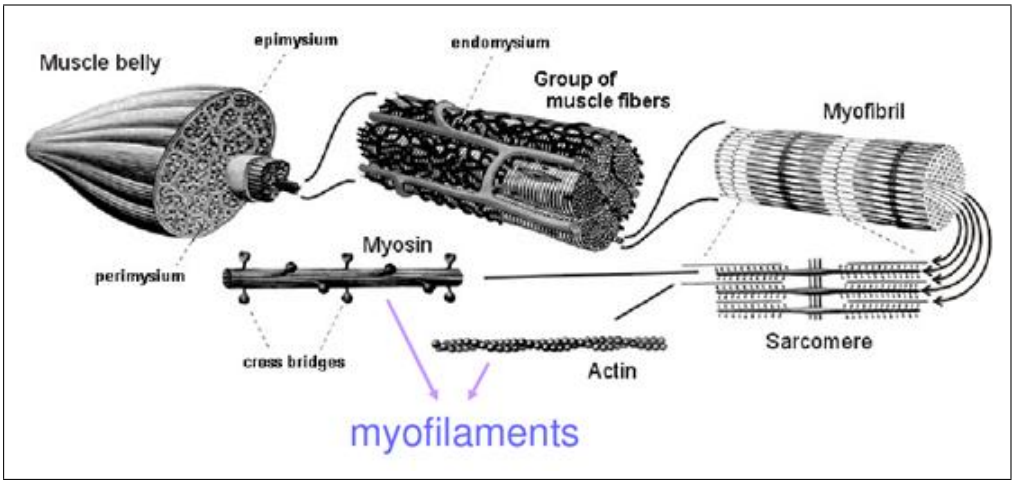

Figure 2.3 Structural units of muscle [3].

2.3.2 Muscle Contraction

Muscles contract and produce force by sliding its filaments and forming cross-bridges. Actin filaments slide over the myosin filaments. The contraction of muscle depends on the presence of ATP and Ca^{2+}. ATP is needed for two things:

- Hydrolysis of ATP is needed for the movement of the myosin head.
- ATP is needed to break the bond between actin and myosin.

Contraction starts with a sufficient impulse. After impulse Ca^{2+} concentration increases in the myoplasm. Ca^{2+} binds to troponin C, which causes the whole troponin complex to retract and to pull the tropomyosin molecule away from the myosin binding site of myosin filament. The myosin head binds to the actin filament.

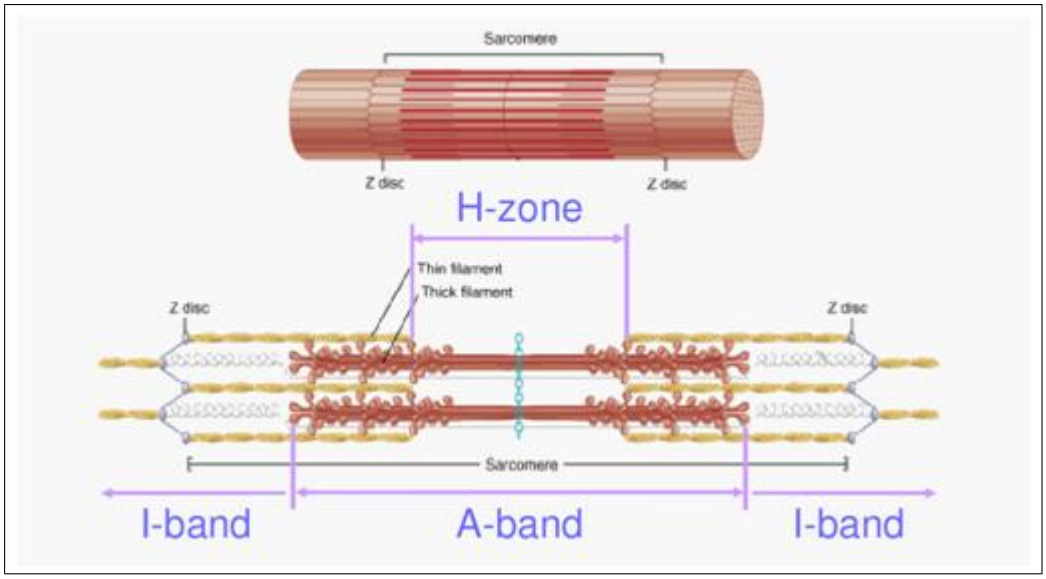

Figure 2.4 The structure of a sarcomere [4].

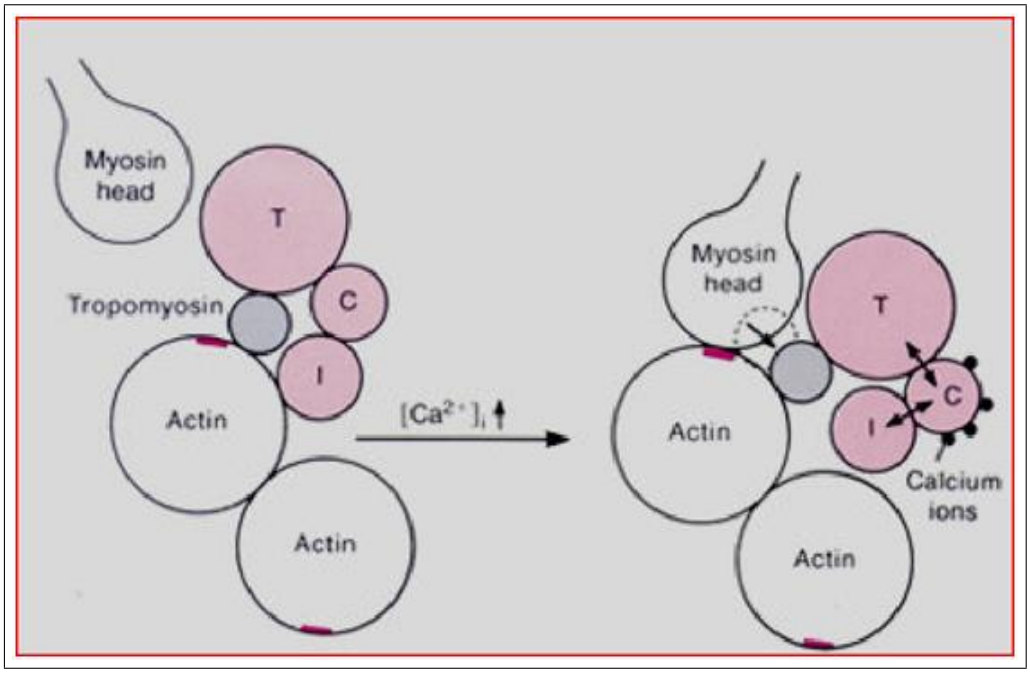

Figure 2.5 Binding of actin filament to myosin filament [4].

With the hydrolysis of ATP the myosin head is turned from a 90° angle, relative to the actin filament, to a 45°angle. This movement results in a sliding of the filaments in relation to each other. When a new Mg-ATP molecule binds to the myosin head, the bond between the two filaments is broken. The energy produced during the binding event between Mg-ATP and myosin is used to turn the myosin head back to its initial 90° angle.

3. OPTICAL IMAGING

Near-infrared spectroscopy uses near-infrared light to detect physiological changes in the muscle and brain. Some substances, chromophores, absorption rates are high enough to make a meaningful measurement by attenuating the transmitted light. A chromophore is particular molecular or compound that absorbs transmitted light in the spectral region of interest.

Substances like water, melanin, and bilirubin the concentration of them stays virtually constant with time. Substances like oxygenated haemoglobin (HbO2), deoxygenated haemoglobin (Hb), and oxidized cytochrome oxidase (CtOx) have changing concentrations in relation to the metabolism [7, 5, 19].

Above the wavelength of 900 nm the absorption of water is very high, for that reason studies are made below 900 nm. Below the wavelengths of 700 nm the absorption of Hb is very high and sets the lower boundary of the studies. Between this limits there is an optical window where sensitive measurement can be made [13, 5].

3.1 Absorption

The Beer-Lambert Law defines the absorption of the light intensity in a non-scattering medium. According to this law the attenuation (A) is proportional to the concentration of the compound in the solution (c) and the optical path-length (d)

$$A = \log_{10}(\frac{I_o}{I}) = a \cdot c \cdot d \tag{3.1}$$

where A is the attenuation measured in optical densities, I_o is the light intensity incident on the medium, I is the light intensity transmitted through the medium, a is the specific extinction coefficient of the absorbing compound measured in micro-molar per cm, c is the concentration of the absorbing compound in the solution measured in micro-molar,

and d is the distance between the points where the light enters and leaves the medium. The product $(a \cdot c)$ is the absorption coefficient of the medium μ_a.

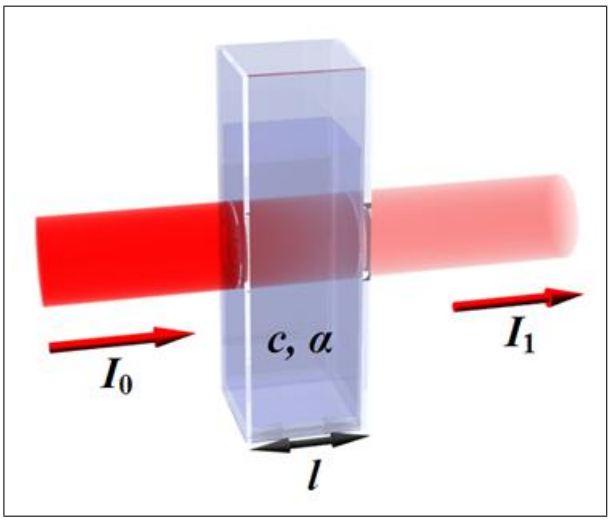

Figure 3.1 A representation of Beer - Lambert law where light passing through a substance and due to absorption of light within the substance the emerging light has a lower intensity [1].

3.1.1 Water

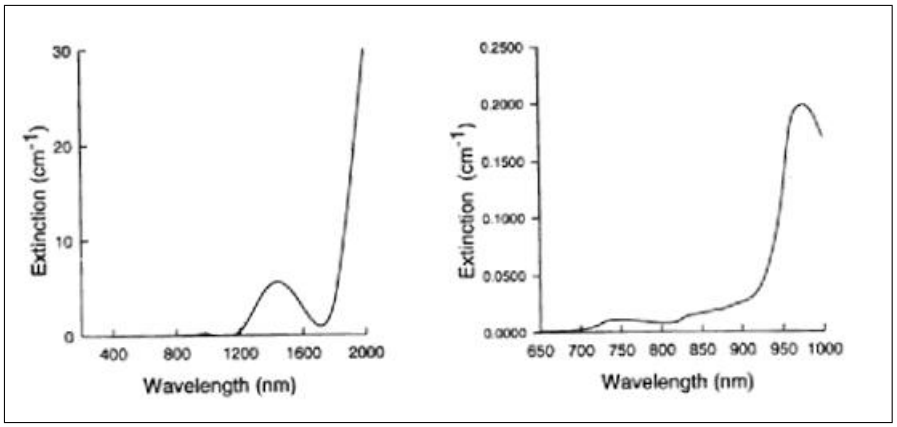

Figure 3.2 The absorption spectra of pure water [5, 6].

The absorption of water below 900 nm is relatively low. After 900 nm the absorption of water increases with increasing wavelength. It reaches a peak at 970 nm [7, 5, 6]. Since the concentration of water in human tissue is very high, the water's optical characteristics determine the wavelength region that can be worked. Because of this limit the depth in tissue which light can reach is limited considerably. In clinical

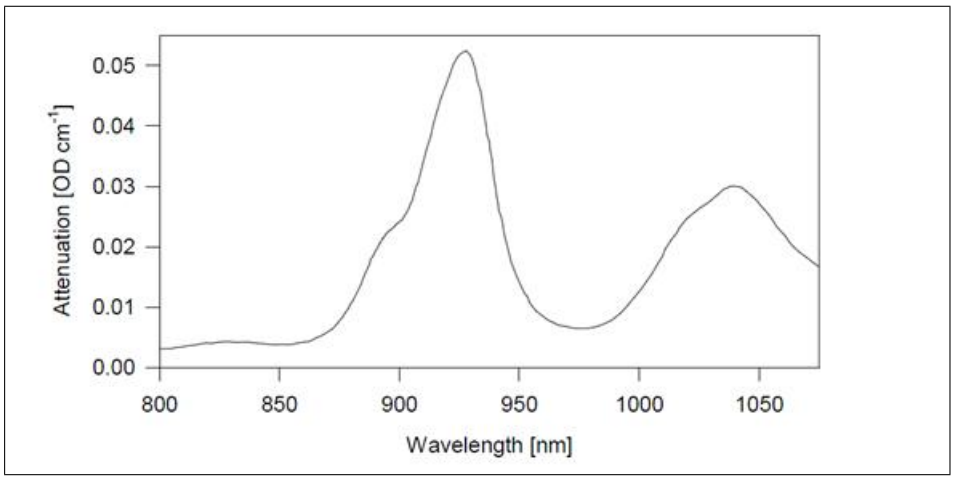

Figure 3.3 The absorption spectra of lipids [6].

measurements the water concentration in tissue can be thought of as constant, and as such water acts as a fixed constant absorber [7, 5, 6].

3.1.2 Lipids

Lipids concentration in the region of interest varies from tissue to tissue and human to human. But it can also be thought of as a constant absorber in clinical measurement. The concentration of the lipid probably won't change during the measurements. The absorption spectrum of lipid is approximately the same as that of water [7, 5, 6].

3.1.3 Melanin

Melanin is found in the epidermis of the skin. At the ultra-violet region of the spectrum the epidermis is very good absorber. This absorption is accepted as constant and not oxygen related. But still the melanin concentration effects the amount of the light reflected from the skin and so the light that is transmitted in to the tissue [7, 5].

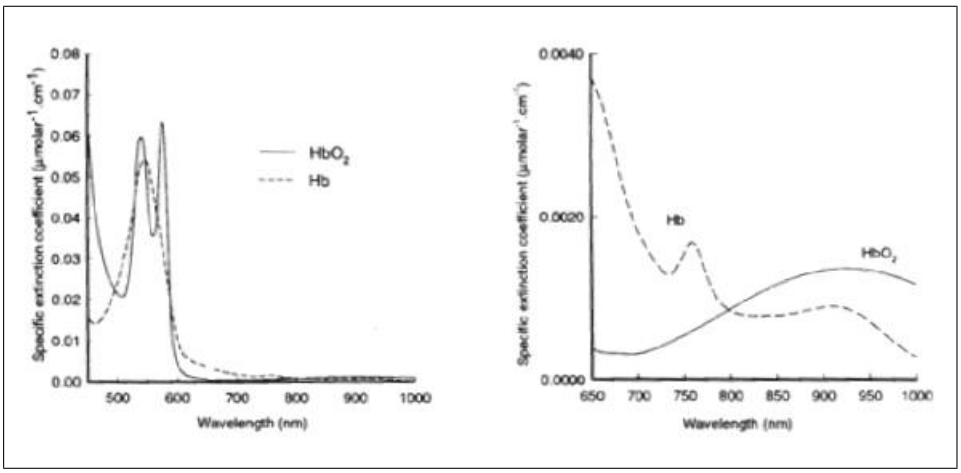

Figure 3.4 The absorption spectra of HbO2 and Hb [5, 6].

3.1.4 Haemoglobin

In the NIR region the absorption rates decreases significantly, but also the absorption characteristic of oxy-Hb and deoxy-Hb are significantly different. This allows them to be detected separately by using several wavelengths. In the visible region as seen from the figure the absorption levels are very high. This is the reason why arterial blood very rich in oxygen looks bright red and venous blood very poor in oxygen looks blue [7, 5, 6].

3.1.5 Scattering

Scattering occurs intracellularly and extracellularly at the boundaries of cell membranes of the cell and the membranes of the organs within the cell. Scatter significantly increases the length of the photon path. And by so scatter increases the abruption amount [7, 5, 6].

3.1.6 Haemoglobin

The direction of the scatter is dependent on the size of scattering particle, the wavelength, and refractive indices of the medium. In the NIR region of the electromagnetic spectrum almost all of the collusions are elastic [6].

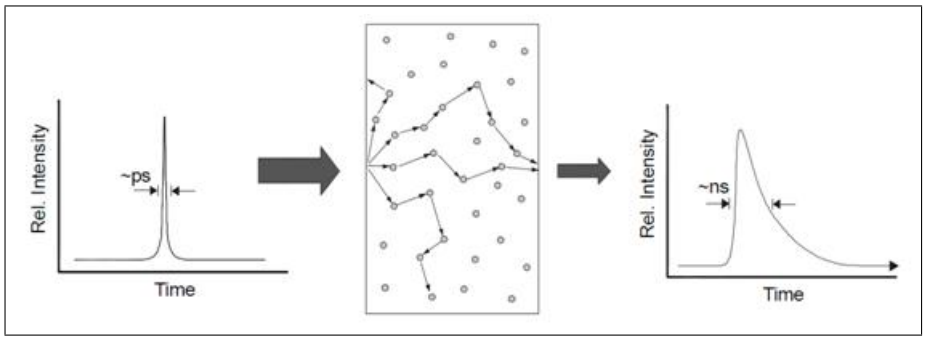

Figure 3.5 Scattering of a photon can be seen in this figure [7].

The attenuation due to single scattering is proportional to the number density of the scattering particles (N), the scattering cross section of the particles (s) and the optical path-length (d):

$$A = \log_{10}(\frac{I_o}{I}) = N \cdot s \cdot d \tag{3.2}$$

The product $N \cdot s$ is known as the scattering coefficient of the medium (micro seconds), and is the probability per unit length of a photon being scattered. Bone, cerebral white matter and skin dermis are the most scattering tissues. Empirically it is shown that light follows a banana shaped path [5, 6].

3.2 The Modified Beer-Lambert Law

In a highly scattering medium the Beer-Lambert relationship need to be changed. These changes are:

- For the scattering losses, G an additive term

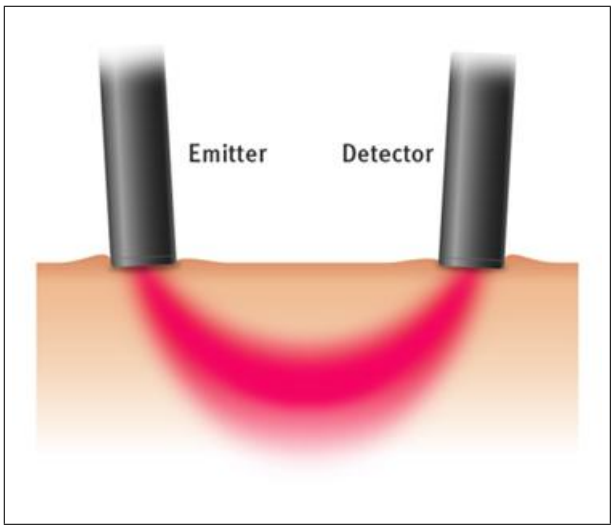

Figure 3.6 Banana shape scatter [2].

- A multiplier, because the optical path-length increase [6].

$$DP = DPF \cdot d \tag{3.3}$$

where d is the geometrical distance, DP is for the differential (true) path-length, and DPF is a scaling factor of DP. And the modified Beer-Lambert law becomes:

$$A = \log_{10}(\frac{I_o}{I}) = a \cdot c \cdot d \cdot DPF + G \tag{3.4}$$

The equation 3.4 can't be solved because G isn't known and also G changes with measurement geometry and scattering coefficient of the tissue being measured. But if G stay unchanged, then a change in concentration of the chromophore from a measured change in attenuation can be measured [6].

$$(A_2 - A_1) = (c_2 - c_1) \cdot a \cdot d \cdot DPF \tag{3.5}$$

3.3 Optical Path-length (DP)

Optical path-length is affected from the tissue type, wavelength of the measurement, absorption coefficient, and the geometry of the optodes [6].

3.3.1 Tissue Type

In the measured tissue the ratio of the soft tissue, muscle and bone and etc. effect the DPF directly. Thus for, a difference is seen in measurements made from various tissues like forearm, calf, and adult head [6].

3.3.2 Wavelength and Absorption Coefficient

From the experiment made with forearm, calf, adult head and infant head it is seen that with increasing wavelength (from 740 to 840 nm) the DPF decreases [6].

3.3.3 Geometry of Optodes

With the help of simulation for a spherical object it is shown that the DPF is dependent on the angular position. Between the emitter-detector angles 180 to 60 degrees the value of DPF can vary significantly, and for lesser angles it may decrease more rapidly. But with experiments it is shown that in all tissues DPF initially falls with increasing geometrical distance, d, and the value becoming almost constant for source-detector spacings above 2.5 cm. This difference happened because the simulation did not considered the inhomogeneity of the tissue [6].

3.4 Methods

3.4.1 Math

To analyze the measurement data recorded from a tissue, mathematical models are used. With these models not only the absorption, also the scattering is analyzed. These models explain how light travels, absorbs, and scatters during the measurements. The most common methods are the Differential Path-length Factor (DPF) and Diffusion Approximation [11].

3.4.1.1 DPF. With DPF method the changes in the concentration of chromophores can be determined. DPF method uses the modified Beer-Lambert Law to explain the behavior of the photon traveling in the tissue. DPF method only measures the light attenuation changes. DPF method is very sensitive to motion artifacts, and behaves the tissue and the change in concentration as if they are homogeneous. Mostly used by the Continuous Wave NIRS [11].

3.4.1.2 Diffusion Approximation. The diffusion approximation is a good tool in analyzing transport of light from a tissue. The diffusion approximation has analytical solutions under the following assumptions:

- Tissue is homogeneous
- Scattering is much larger than absorption
- The tissue has a specific geometry-infinite, semi-infinite, slab, or two-layered [11].

The diffusion approximation can be used to measure absolute values of the absorption and scattering coefficients of tissue and from the absorption coefficient, absolute values of the chromophore concentration can be calculated [11].

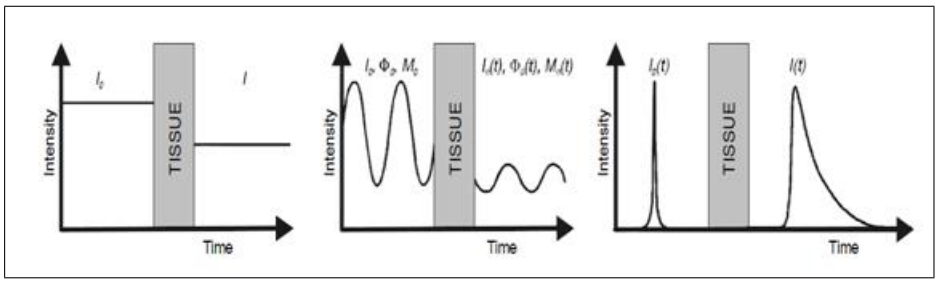

Figure 3.7 Types of NIRS, Representations: at the left Continuous Wave, at the middle Phase modulation Spectroscopy, and at the right Time Resolved Spectroscopy [7].

3.4.2 Ways of measurement

The most widely used of techniques are Continuous Wave (CW), Time Resolved Spectroscopy (TRS), and Phase Modulation Spectroscopy (PMS). CW is not method that gives absolute measurements of the concentration, but it requires less complicated systems and so it is cheaper and more easily produced. TRS and PMS can give absolute measurements of the concentration within the tissue of interest [11].

3.4.2.1 Continuous Wave (CW). In the continuous wave the intensity of the light is measured. By using CW low-cost, compact devices can be manufactured. Both lasers and light emitting diode can be used in this technique. CW is reliable technique and gives enough results to see the functional activity. The disadvantage of CW is measurement errors occurs due to motion artifacts [11].

3.4.2.2 Spatially Resolved Spectroscopy (SRS). SRS measures the intensity of the light by measuring different source detector distances. SRS techniques assume that the coupling is the same for the different source-detector distances and, by measuring the intensity as a function of the distance, determine a parameter that is independent of the coupling [11].

3.4.2.3 Time Resolved Spectroscopy (TRS). TRS systems usually give a pulse of light that is less than 100 ps and measure the time of flight and intensity of the light. By using this method the absolute value of the concentration being measured can be calculated. The result gathered is used to produce a histogram showing the arrival time verses the number of photons arrived. This method is very sensitive to noise since this technique involves a small amount of photons in relation to the other techniques [11].

3.4.2.4 Phase Domain Spectroscopy (PMS). PMS Is also called frequency domain spectroscopy. PMS systems use frequency modulation and send the light into the tissue with more than one frequency. Time of flight can be measured from the phase difference of the entering and exiting signals [11].

3.4.2.5 Broadband Imaging. Broadband imaging uses white light instead of near-infrared light. Transmitted light contain information about the whole spectrum. This makes the chromophores discrimination to be more effective [11].

3.4.2.6 Diffusing-wave spectroscopy (DWS). DWS uses lasers with long coherence length. When light enters to a tissue, it scatters and photons go different direction. At some point some photon path crosses. This results in a speckled pattern which changes due to change in concentration of chromophores of the tissue of interest [11].

3.4.2.7 Near Infrared Imaging (NIRI). NIRI is also called diffuse optical imaging (DOI) because it produces two dimensional images of the chromophore concentration via DWS.

3.5 Devices

There are many available NIRS clinical devices that are commercially available, and so many is developed or being developed. At table 3.1 the commercial NIR clinical instruments is listed [11].

In the photometers the number of channels goes up 96 channels. Mostly single distance CW devices are used. In the oximeters generally multi-distance technique is used. Generally oximeters are made with 2 channels, and number of channels in some types reaches to 4. For imagers minimum 4 and up to 128 channels are used. Mostly CW technique is used [11].

At table 3.2 recently developed near infrared prototypes are listed. As seen from the table mostly CW and TRS is developed. Number of channels rises to 300.

3.5.1 NIROXCOPE

NIROXCOPE system is one of the recently developed prototypes. NIROXCOPE is developed at Boğaziçi University by Ata Akın. At figure 3.8 a picture of the system is shown. This system uses four leds, and 10 detectors and requires external control. But due to multiplexing it works as if there are 16 detectors. NIROXCOPE is a continuous wave fast optical imager [5].

NIROXCOPE system uses multi-wavelength leds. Every led has 12 leds embedded inside, 4 leds that emits 730 nm, 4 leds that emits 805, and 4 leds that emit 850 nm. NIROXCOPE system operates in the time multiplexed and wavelength multiplexed modes [5].

In wavelength multiplexed mode it operates by interchanging active leds groups of different wavelengths, and in time multiplexed mode it changes the active detector groups. At first quadrant it activates the first leds 730nm leds of the led and the

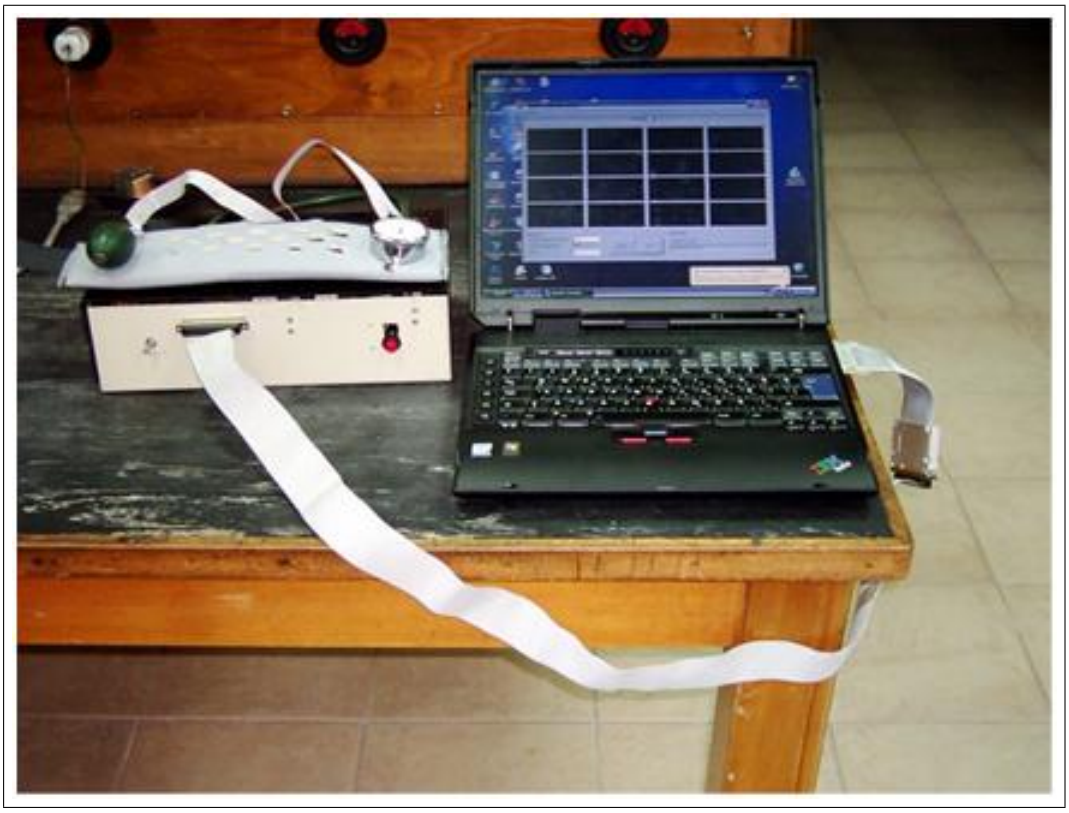

Figure 3.8 NIROXCOPE, the CW Functional Optical Imager [5].

detectors around it, then at second quadrant the first leds 805 nm leds are activated and the detectors around them, at third quadrant the first leds 850 nm leds and the detectors around them are activated, at fourth quadrant the second leds 730 nm leds are activated and so on.

3.5.2 Comparison of the NIRS Devices

NIROXOCOPE is a relatively slow system. NIROXOCOPE works in cycles of ons and offs. The system designed at this study increases the speed of data collection, and by eliminating the need for the multiplexers, and making the system simpler. Also NIROXOCOPE is affected from electromagnetic interference. By using different wavelengths, the electromagnetic interface will be decreased and the signal to noise ratio of the signal will be increased.

Table 3.1
Commercial Near Infrared Clinical Instrumentation [11].

Instrument	Technique / Number of channels	Company
BOM-L1 TR	Single-distance CW / 1	Omegawave, Japan
HEO-200	Single-distance CW / 1	OMRON, Japan
Micro-RunMana	Single-distance CW / 1	NIM, Inc., USA
OXYMON MkIII	Single-distance CW / 1 to 96	Artinis, The Netherlands
FORE-SIGHT	Multidistance / 1	Casmed, USA
INVOS 5100C	Multidistance / 2 or 4	Somanetics, USA
InSpectra 325	Multidistance / 1	Hutchinson, USA
NIMO	Multidistance / 1	NIROX, Italy
NIRO-100	Multidistance / 2	Hamamatsu, Japan
NIRO-200	Multidistance / 2	Hamamatsu, Japan
O2C	Broadband / 2	LEA, Germany
ODISsey	Multidistance / 2	Vioptix, Inc., USA
OM-220	Multidistance / 2	Shimadzu, Japan
OxiplexTS	Multidistance PMS / 1 or 2	ISS, USA
TRS-20	Multidistance TRS / 2	Hamamatsu, Japan
Dynot	CW / up to 32	NIRx, USA
ETG-4000	CW / 44	Hitachi, Japan
ETG-7000	CW / 72	Hitachi, Japan
Imagent	PMS /up to 128	ISS, USA
LED IMAGER	CW / 16	NIM, Inc., USA
nScan D1200	CW / 16 to 32	Arquatis, Switzerland
nScan W1200 Wireless	CW / 16	Arquatis, Switzerland
NIRO-200	CW / 8	Hamamatsu, Japan
NIRS 4/58	CW / 4 or 58	TechEn, Inc, USA
OMM-2001	CW / 42	Shimadzu, Japan
OMM-3000	CW / 64	Shimadzu, Japan

Table 3.2
Main recently developed near-infrared prototypes [11].

Name or City	Technique / Number of channels	University or Firm
Irvine	Broadband PMS / 1	Irvine Univ., USA
Keele	PMS / 1	Keele Univ., UK
Koblenz	Broadband SRS / 1	Koblenz Univ., Germany
NeoBrain	CW / 8	Helsinki Univ., Finland
Philadelphia	Multidistance SRS / 1	NIM, Inc., USA
IRIS-3	CW / 1	INFM, Italy
TSNIR-3	Multidistance SRS / 1	Tsinghua Univ., China
Zurich	PMS / 1	Univ. Hospital Zurich, Switzerland
Arlington	CW / 64	Univ. of Texas, Arlington, USA
Berlin	CW / 22	Charité, Germany
London	CW / 20	Univ. College London, UK
NIROXCOPE 201	CW / 16	Boğaziçi Univ., Turkey
Nanjing	CW / 16	Southeast Univ., China
New York	CW / var.	Columbia Univ., USA
Philadelphia	CW / 16	Drexel Univ., USA
St. Louis	CW / 300	Washington Univ., USA
Zuricha	CW / 16	Univ. Hospital Zurich, Switzerland
Boston	TRS / 32	Harvard Univ., USA
Hamamatsu	TRS / 16	Hamamatsu, Japan
Milan	TRS / 16	Politecnico of Milan, Italy
Monstir	TRS / 32	Univ. College London, UK
Strasbourg	TRS / 8	Strasbourg Univ., France
Warsaw	TRS / 16	Academy of Sciences, Poland
Helsinki	PMS / 16	Helsinki Univ., Finland
Seoul	PMS / 16	Yonsei Univ., South Korea
Hokkaido	SRS / 64	Hokkaido Univ., Japan
Irvine	SRS / CCD	Irvine Univ., USA

4. Design

This Master of Science thesis is focused on developing a near infrared spectroscopy device, an optical imager, using continuous wave spectroscopy method. The instrument designed and the details are given in this chapter. The instrument takes continuously measurements by feeding the leds of different wavelength characteristics with sinusoidal signals with different frequencies.

4.1 Design Considerations

In this thesis, the goal is to development of an optical imaging system used to measure muscle oxygenation, the changes in oxy-Hb and deoxy-Hb concentrations, in Turkey. The optical imager must have an emitter part and a detector part on a probe. The system should also have a signal generator part, filtering part, and peak detection part.

4.1.1 Needs

4.1.1.1 Probe. The probe has to house leds that are capable of emitting light at the near-infrared spectrum, because within the optical window at 730 nm the concentration changes of deoxy-Hb and at the 850 nm the concentration changes of oxy-Hb can be monitored. The detectors should be capable of detecting light at the near-infrared spectrum. The detectors should be capable of detecting low level signal to be able to shoe the changes of the concentration of the chromophores of interest.

4.1.1.2 Signal Generation. The signal generator part should produce two sinusoidal signals with two different frequencies. Each signals should be fed to one of the leds, other signal to the leds with different wavelength emission so that the light in-

tensity will change accordingly and the measurements of the both wavelengths can be made at the same time.

4.1.1.3 Filtering. The detectors collect both of the responses of the different wavelengths. The gathered response from the tissue of interest will be filtered and so differentiated. This needs two band-pass filters with different cutoff frequencies.

4.1.1.4 Peak Detection. The transmitted signal losses most of its energy. Thus the amplitude of the detected signal is very low. For signal processing the amplitude of the signal should be increased via amplification. Also the response of the system is encoded on the input sinusoidal signal should be gathered. For that an peak detector is needed.

4.1.2 System Specifications

- The optical imager designed should consume low power, it could be able to be operated with batteries
- The optical imager designed should be low cost.
- The optical imager designed should be portable, and should allow clinical trials.

4.2 System

This instrument is based on the Uzay Emrah Emir. Uzay Emrah Emir designed a CW optical imager at Boğaziçi University, Turkey and discussed in the third section.. The instrument designed has six parts:

This instrument feeds the leds with the same dc voltage and the changes the intensity of the light by a sinusoidal signal. The near-infrared light is produced by

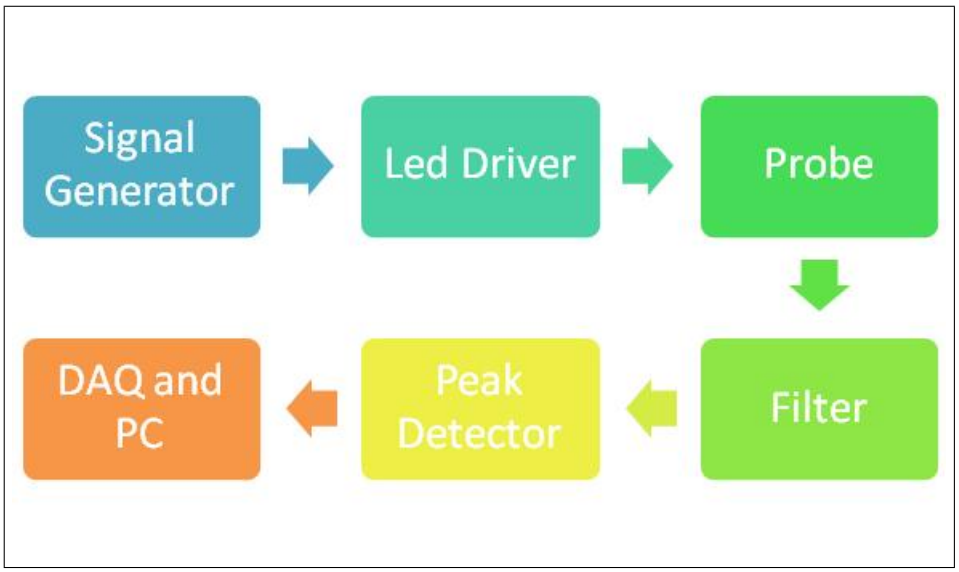

Figure 4.1 Parts of the instrument designed.

leds and transmitted to the tissue of interest. The transmitted light is collected by near-infrared sensitive detectors and passed through filters. Then the output signal is acquired, passed from the peak detector and collected with a DAQ card and personal computer.

4.2.1 Signal Generator

To be able to record simultaneously from the both of the wavelengths the leds with different wavelengths are fed with different frequencies. For this reason we use, two different frequencies, 1.7 kHz and 3.0 kHz. These are generated by the ICL8038, Precision Waveform generator/Voltage Controlled Oscillator. The ICL8038 is chosen due to several reasons. ICL8038 is:

- Low distortion
- Simple and easy use
- Wide range of frequency to operate
- Low frequency drift with temperature

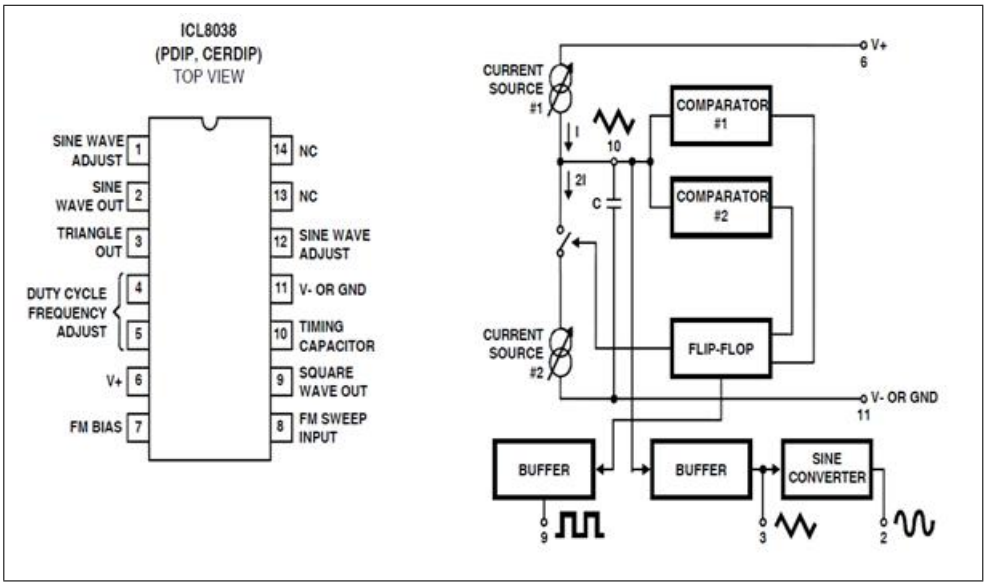

Figure 4.2 ICL8938 Voltage controlled oscillator. This oscillator can give a sinusoidal, triangular or square wave from 0.001Hz to 300 kHz by the help of a few passive components. Second pin gives a sinusoidal wave output, third pin gives out a triangular wave output, and the ninth pin give out a square wave output [8].

While using the ICL8038 at the sinusoidal wave mode lover than 1 percent distortion can be achieved. ICL8038 can be operated between frequencies 0.001 Hz to over 300 kHz. The frequency is set by a two resistors and a capacitor. And the frequency drift with temperature is low, $250 ppm/^oC$ [8].

In the instrument two voltage controlled oscillators are used. The frequency (f) is set by the two equal resistors (R) to the 4th and 5th pins, and a capacitor (C) to the 10th pin by the formula [8]:

$$f = \frac{0.33}{(R \cdot C)} \tag{4.1}$$

In figure 4.4 there are two circuits for generating two different frequencies to feed the leds with different wavelengths are seen. First circuitry seen in the above gives the Sinus Out1 wave with the 1.6 kHz sinusoidal signal by using 18 kohm resistors and a 10 nF capacitor. Second one seen below gives Sinus Out2 wave with 3.0 kHz by using 10 kohm resistors and a 10 nF capacitor. The amplitude of the signal is adjusted with the 100 kohm potentiometers RP1 and RP2. As the operational amplifier LM324 low power quad operational amplifier is used. The output of ICL8038s is seen in figure 4.4.

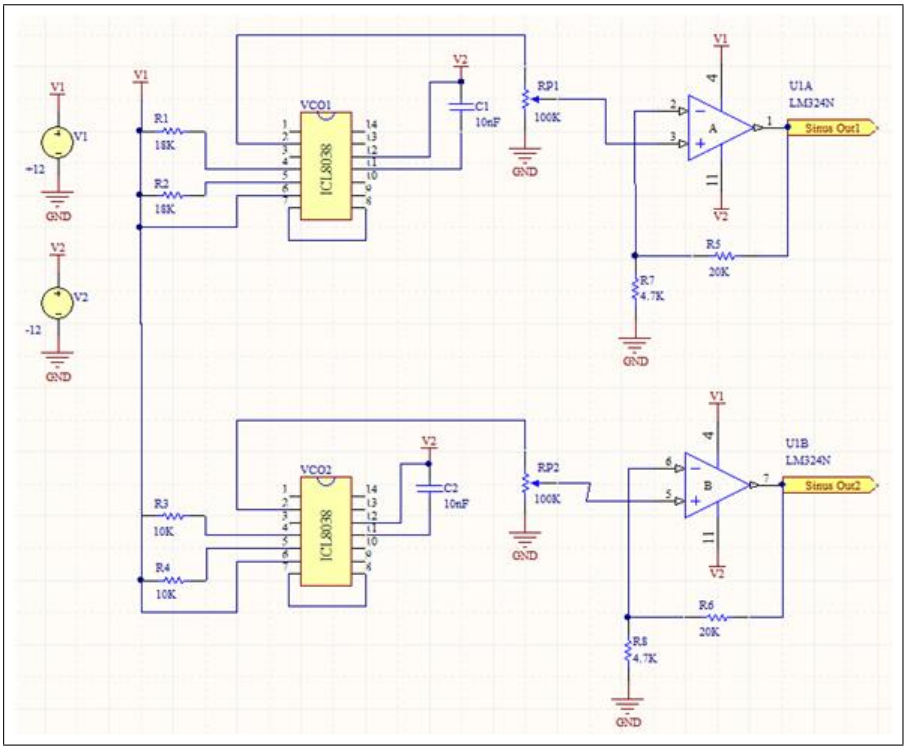

Figure 4.3 Circuitry used for signal generation. Two circuits are used feed the leds with sinusoidal signal with two different frequencies. Second pin of the ICL8038 is used because the second pin gives out a sinusoidal output. The latter circuitry is for adjusting the amplitude of sinusoidal signal.

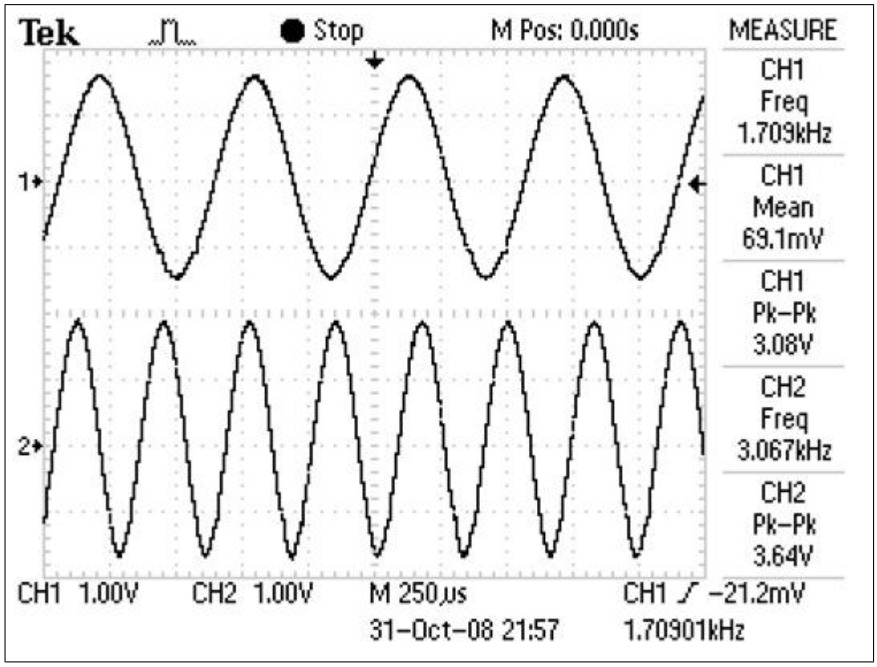

Figure 4.4 The output of the ICL8038 waveform generator from the instrument recorded by Tektronix Digital Oscilloscope. The first channel shows the 1.7 kHz signal and the second channel show the 3.06 k Hz signal.

4.2.2 Led Driver

Table 4.1
For the led group that emits 850nm, the currents measured and corresponding offset voltages.

V_{offset} (V)	$I_{led(dc)}$(mA)
0,00	0,00
1,00	8,40
2,00	17,60
3,00	26,20
4,00	36,20
5,00	45,40
6,00	50,80
7,00	50,80
8,00	50,80
9,00	50,90
10,00	50,90
10,90	50,80

To be able to observe the changes in the haemoglobin concentration changes, the intensity of the light emitted by the leds should be constant with time. To keep the current that passes from the leds constant a led driver circuit is used.

In the led driver as transistor BD135 NPN power transistor and as amplifier LM324 low power quad operational amplifier is used. Since the V1, led voltage drop and transistor voltage drops are nearly constant, by only changing the input of the amplifier the output voltage and so the current that passed through the leds are adjusted. And if the input is constant then the current that passes the leds will be kept constant. In figure 4.9 the whole circuit for led driver part can be seen.

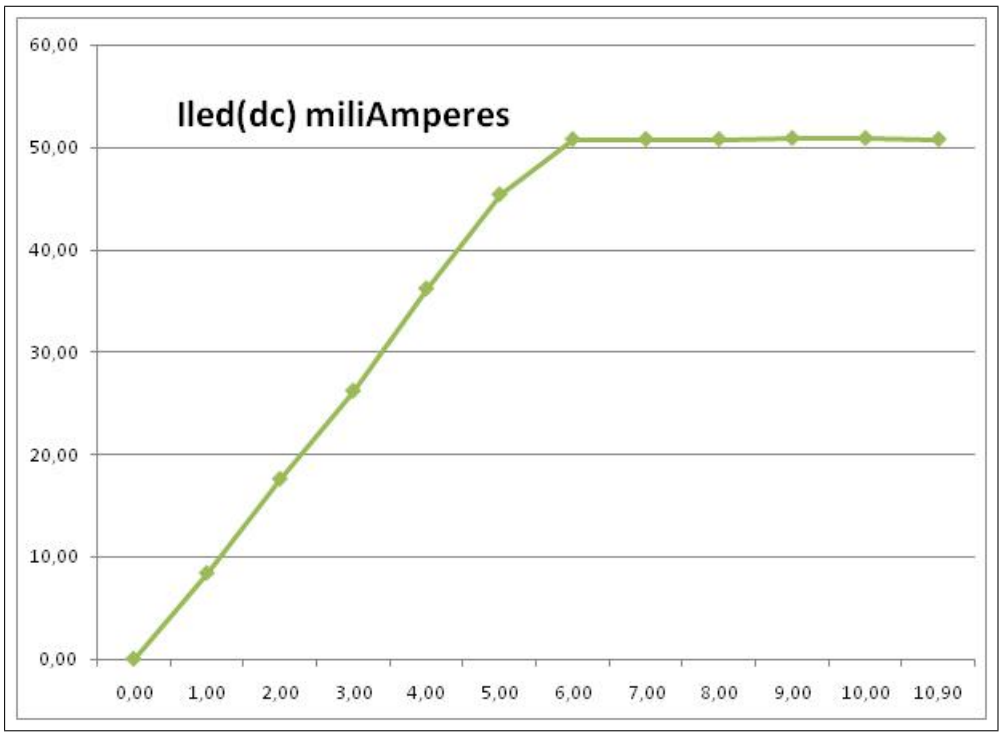

Figure 4.5 The current level verses the corresponding offset voltages are shown for no ac voltage condition.

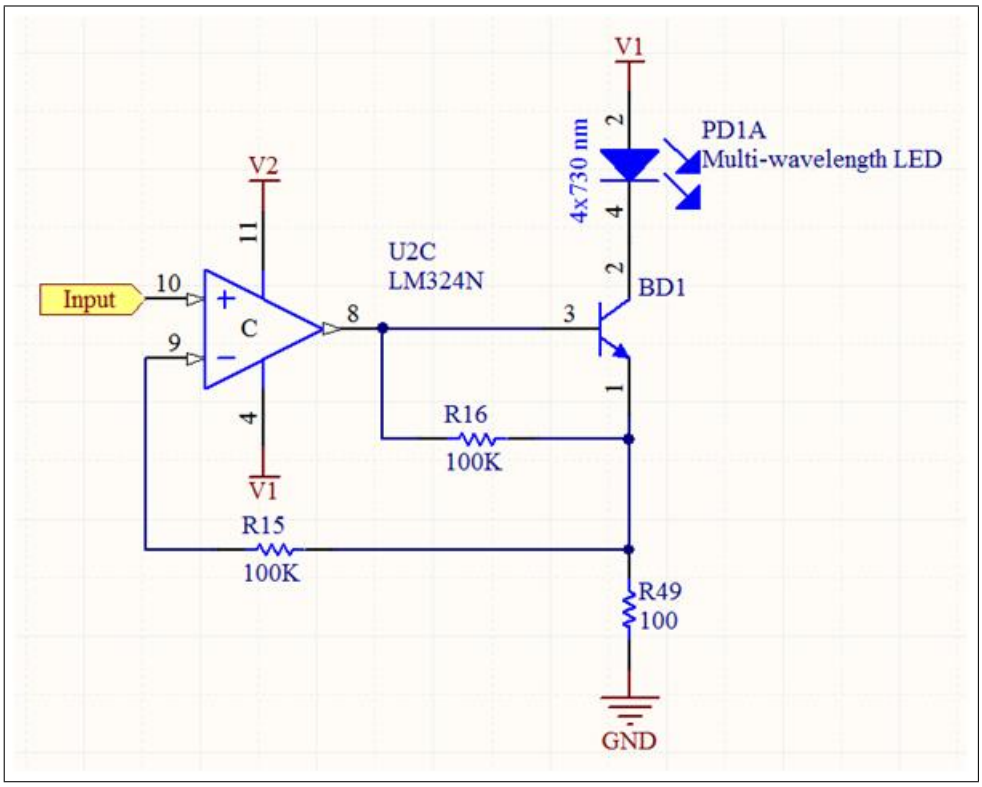

Figure 4.6 The led driver that keeps the current that passes from the led constant. Input cannot exceed 5 V.

Table 4.2
For the led group that emits 850nm, the currents measured and corresponding offset voltages.

V_{offset} (V)	$I_{led(dc)}$ (mA)	$I_{led(ac)}$ (mA)
0.00	0.03	4.56
1.00	9.09	4.66
2.00	17.73	4.69
3.00	26.60	4.77
4.00	36.45	4.80
5.00	45.49	4.74
6.00	50.80	0.55
7.00	50.96	0.02
8.00	50.76	0.02

Table 4.3
For the led group that emits 850nm, the currents measured and corresponding offset voltages.

V_{p-p} (V)	$I_{led(dc)}$ (mA)	$I_{led(ac)}$ (mA)
0	25.18	0.02
1.12	25.51	2.94
2.08	25.51	5.74
3.04	27.16	9.5
4.08	26.41	11.71
5.04	26.27	14.84

Empirically it is shown that the current through the leds are constant when the led driver is used, and in the figure 4.6, 4.7, and 4.8 for the given input the current levels are shown; and the tables 4.1, 4.2, and 4.3 shows the values measured during experiment. The table 4.1 lists the current corresponding to an offset voltage given to the led driver, the currents are measured form the 850 nm led group under the condition that the sinusoidal signals generated are not given to the system, and figure 4.6 shows them graphically. In the tables 4.2, and 4.3 the sinusoidal signals generated are present. In table 4.2 the measurements are taken under the condition that sinusoidal input is constant and can be seen in figure 4.7 where as in table 4.3 the measurements are taken under the condition that the offset voltage is kept constant and can be seen in figure

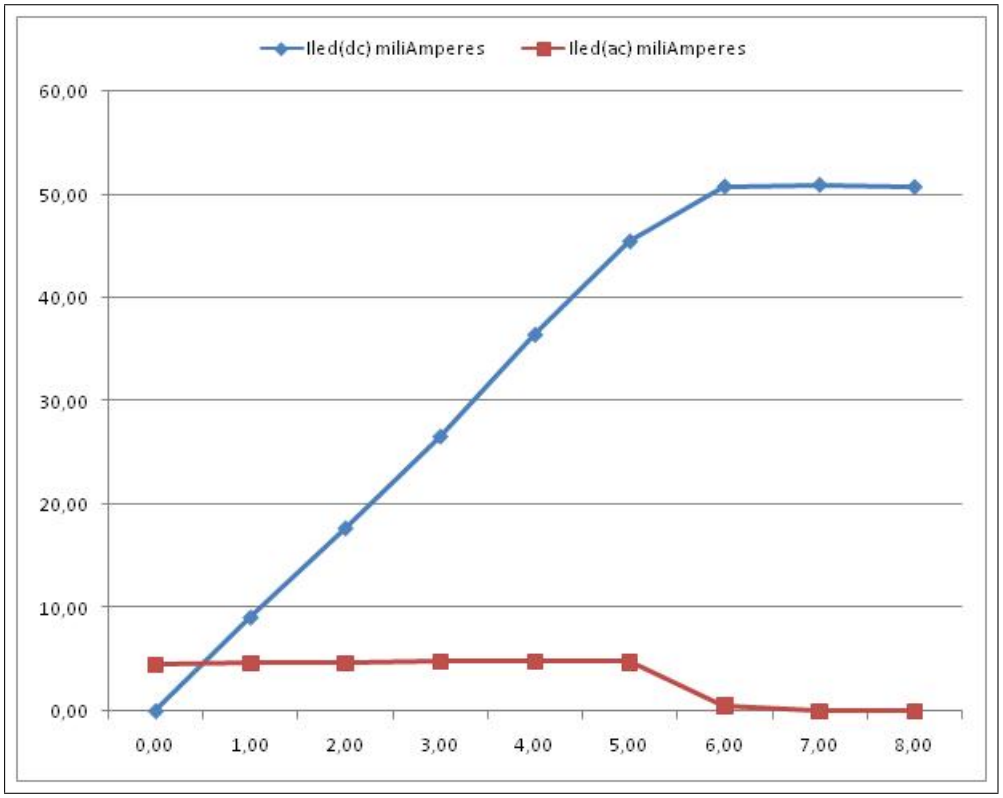

Figure 4.7 The current level verses the corresponding offset voltages are shown for constant ac voltage condition.

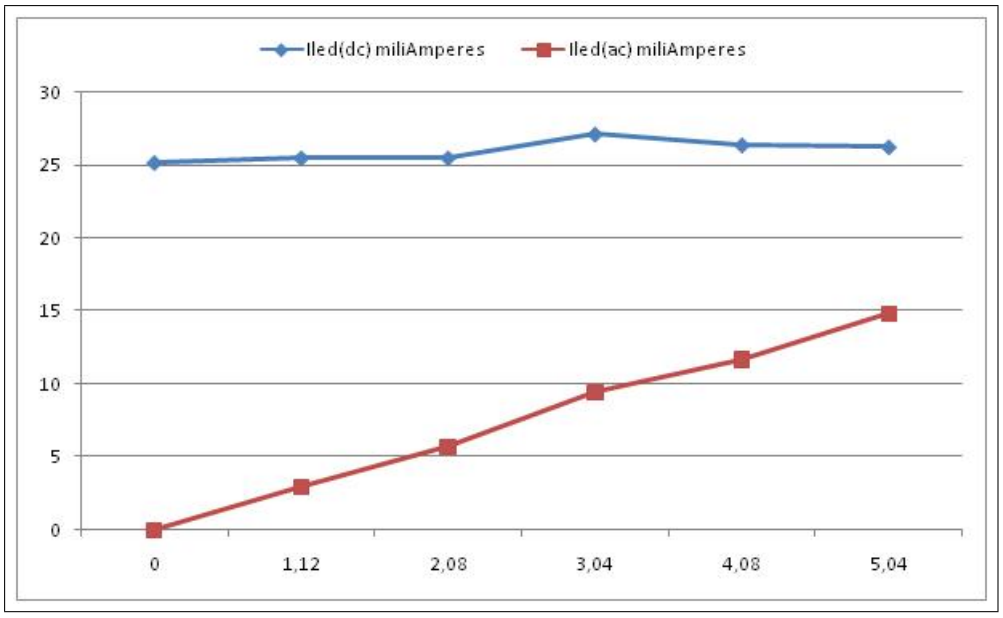

Figure 4.8 The current level verses the corresponding offset voltages are shown for constant dc voltage condition.

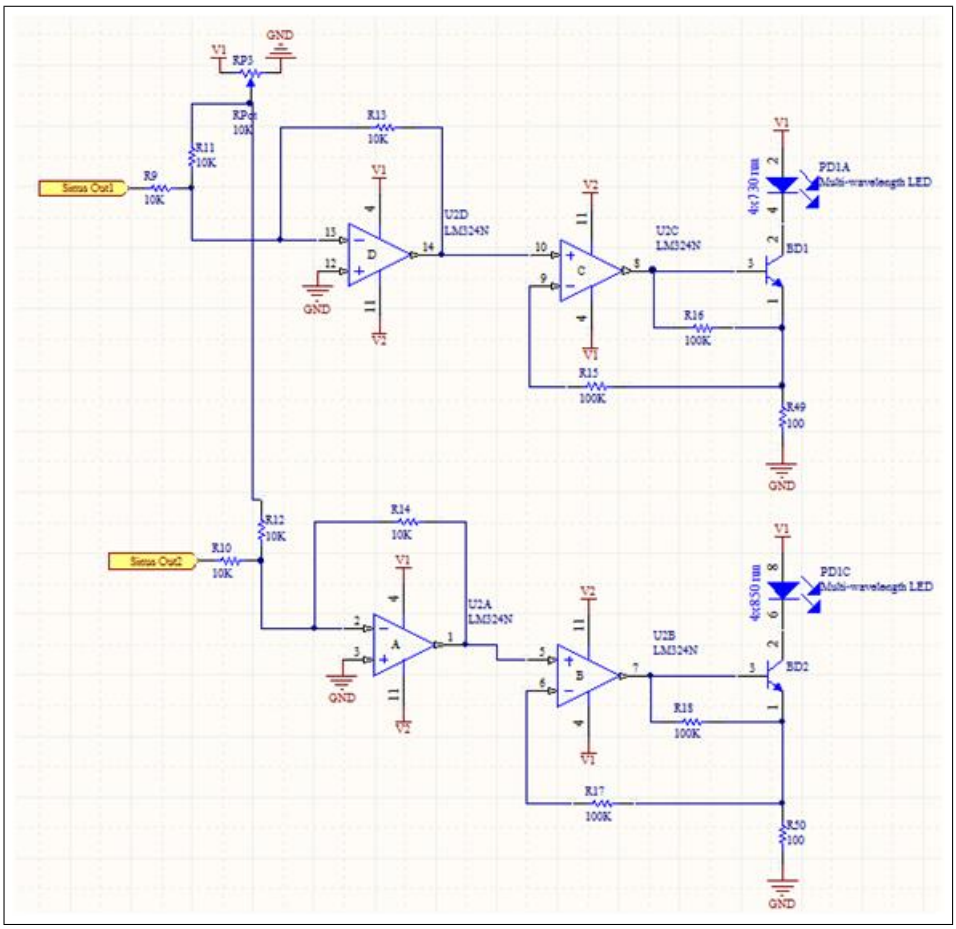

Figure 4.9 The circuitry of the led driver part.

4.8.

4.2.3 Probe

The probe house a single multi-wavelength led that contains 12 leds embedded inside and 2 detectors. The led is the L4X730-4X805-4X850-40Q96-I model stem type led of Epitex, that can emit three different wavelengths at the same time.

The multi-wavelength led contains 12 leds designed in a 4x3 matrix which can be seen from Figure 4.10. Between pins 2 and 4, there are four leds that emits 730 nm near-infrared light. Between pins 8 and 6, there are four leds that emits 850 nm near-infrared light. The leds heating problem is solved with a cooler made from a metal

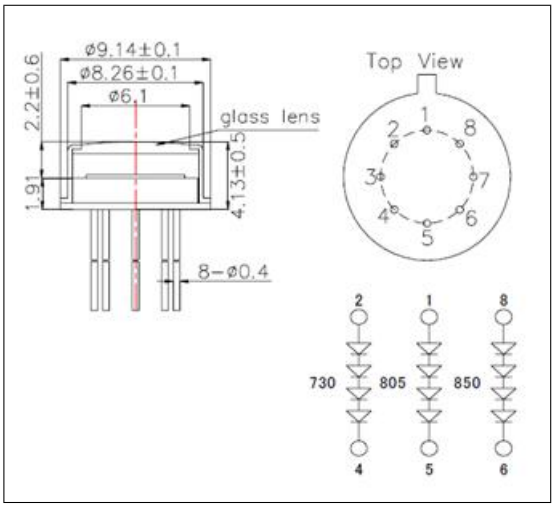

Figure 4.10 The multi-wavelength led of Epitex [9].

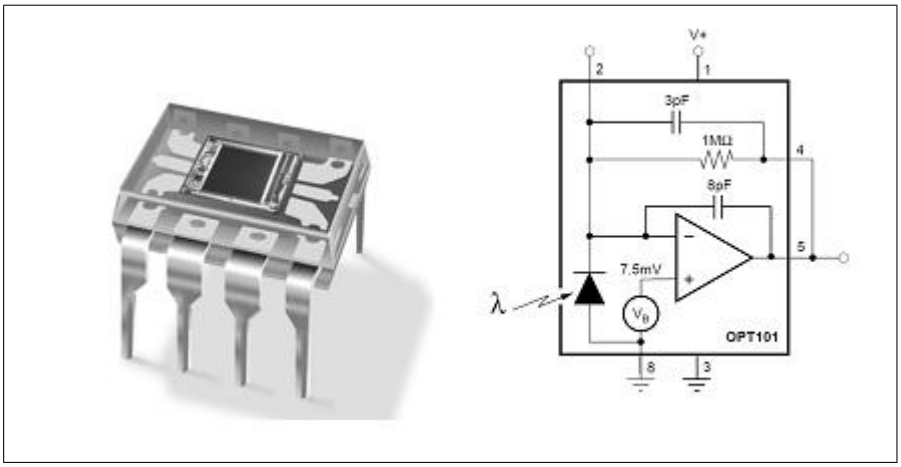

Figure 4.11 The OPT101 OPT101 Monolithic Photodiode and Single-Supply Transimpedance Amplifier [10].

placket. The leds heated up to 50 ^oC and managed to be cooled down to 36-37 ^oC.

The detectors that are used are OPT101 Monolithic Photodiode and Single-Supply Transimpedance Amplifier of Texas Instruments. OPT101 contains a 5.23 mm2 chip and sensitive to a wide range of input light. Peak sensitivity is 700 nm and 950 nm which makes it ideal for the instrument designed. It also has a built in transimpedance amplifier.

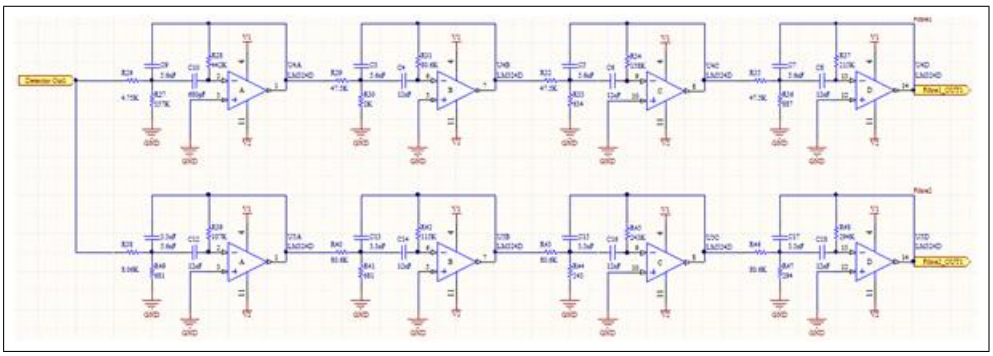

Figure 4.12 The band-pass filters used in the system.

4.2.4 Filter

The two led is driven with different frequencies and constant dc voltage at the same time as seen from figure 4.9. In the tissue both signals add up, because of that the detectors detect both of the signals (see figure 4.13). To differentiate these signals for each detector two band-pass filters are used. The filters used are shown in figure 4.12.

The frequency characteristics of the filters are shown in figure 4.14. The first filter has $f_l = 1400$ Hz and $f_h = 2000$ Hz as the lower and higher cutoff frequencies. The frequency characteristics of the filters are shown in figure 4.15. The second filter has $f_l = 2700$ Hz and $f_h = 3300$ Hz as the lower and higher cutoff frequencies.

The response to the inputs of 2.776 KHz, 1.626 KHz, 1.188 KHz the figure 4.16 , 4.17, 4.18 respectively shows the output of the filters on channel 1 and inputs on channel 2 for the band-pass filter that has the pass-band in between 1400-2000 Hz.

The response to the inputs of 3.625 KHz, 2.888 KHz, 2.362 KHz the figure 4.19, 4.20, 4.21 respectively shows the output of the filters on channel 1 and inputs on channel 2 for the band-pass filter that has the pass-band in between 2700-3300 Hz.

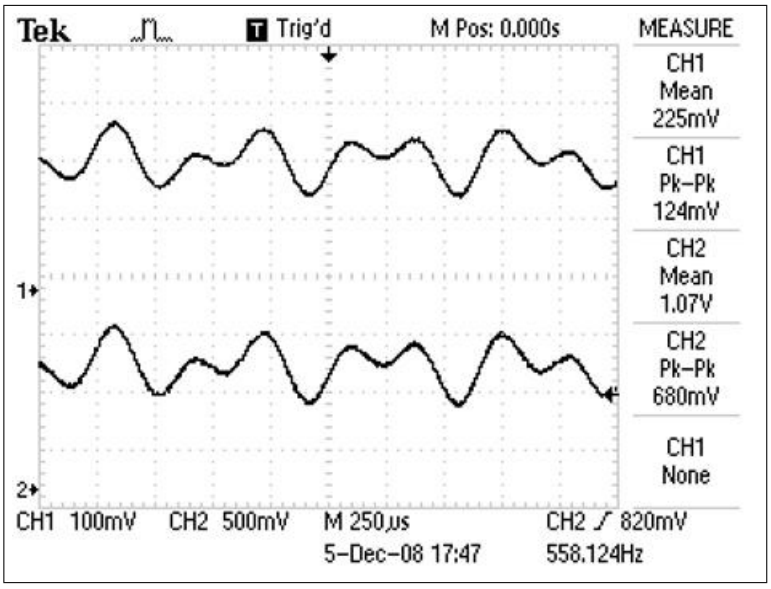

Figure 4.13 The output of detectors from a phantom.

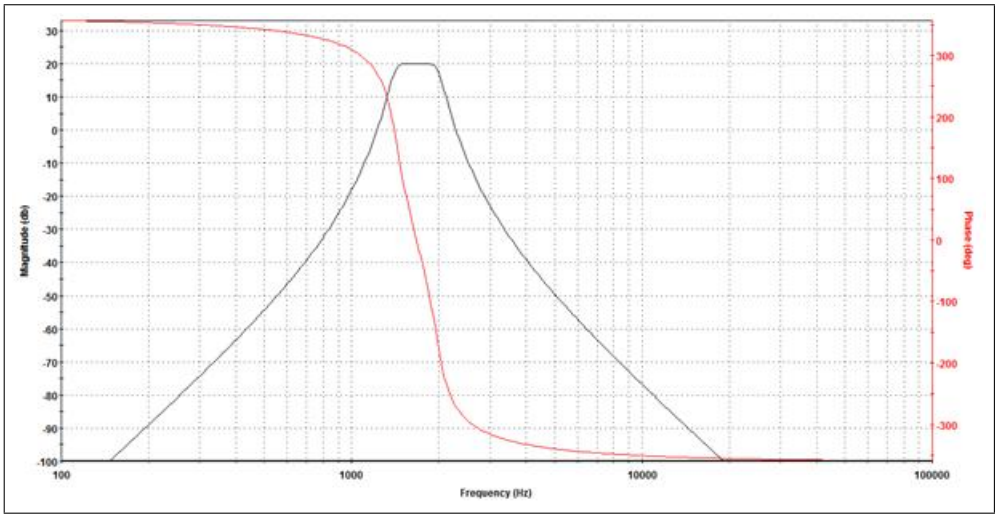

Figure 4.14 The frequency characteristics of the filter with $f_l = 1400$ Hz and $f_h = 2000$ Hz

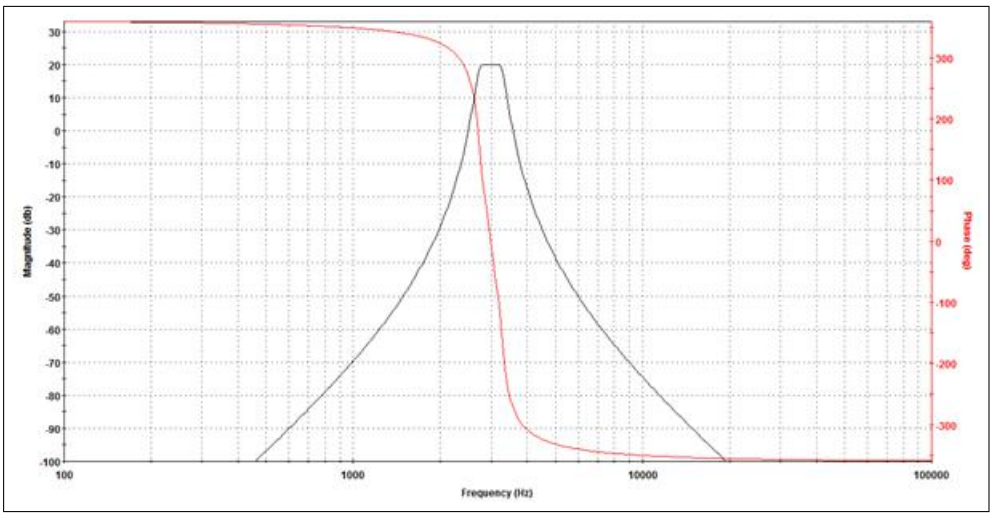

Figure 4.15 The frequency characteristics of the filter with $f_l = 2700$ Hz and $f_h = 3300$ Hz

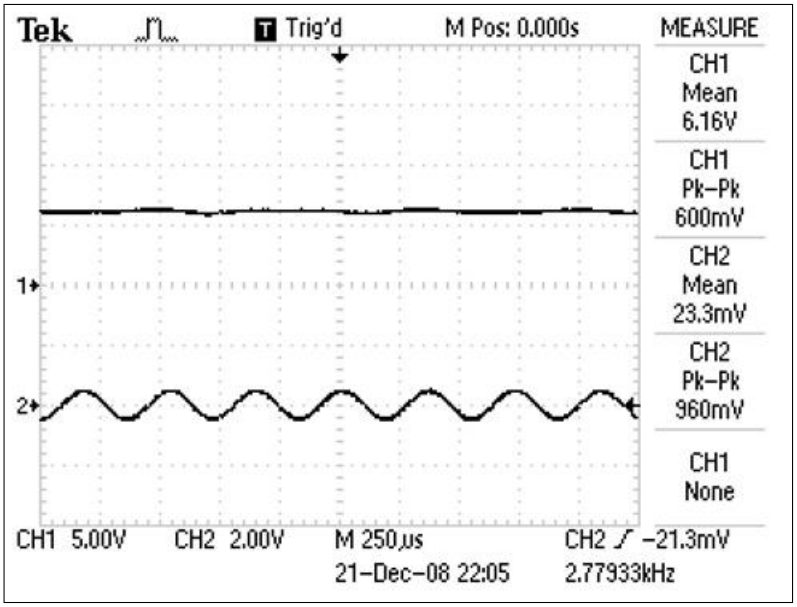

Figure 4.16 For 2.776 KHz input, the response of the first filter (pass-band: 1400-2000, channel 2 input, channel 1 output)

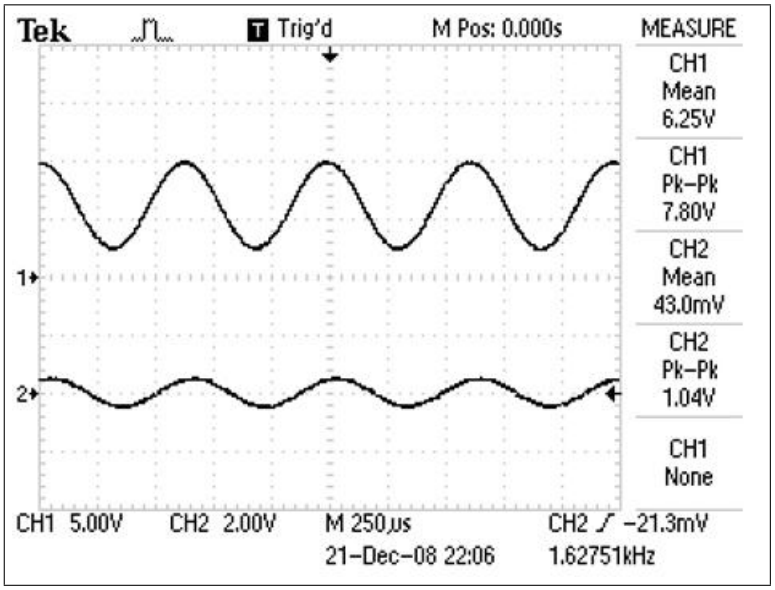

Figure 4.17 For 1.626 KHz input, the response of the first filter (pass-band: 1400-2000, channel 2 input, channel 1 output)

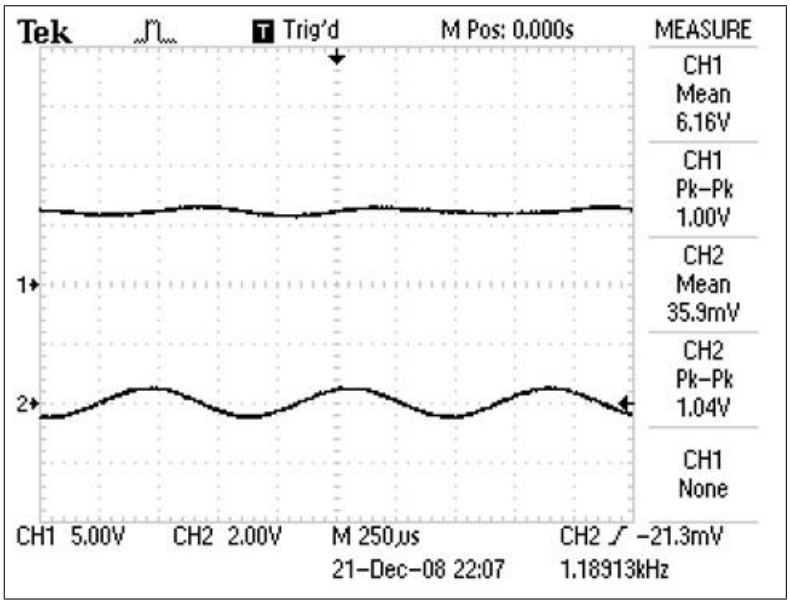

Figure 4.18 For 1.188 KHz input, the response of the first filter (pass-band: 1400-2000, channel 2 input, channel 1 output)

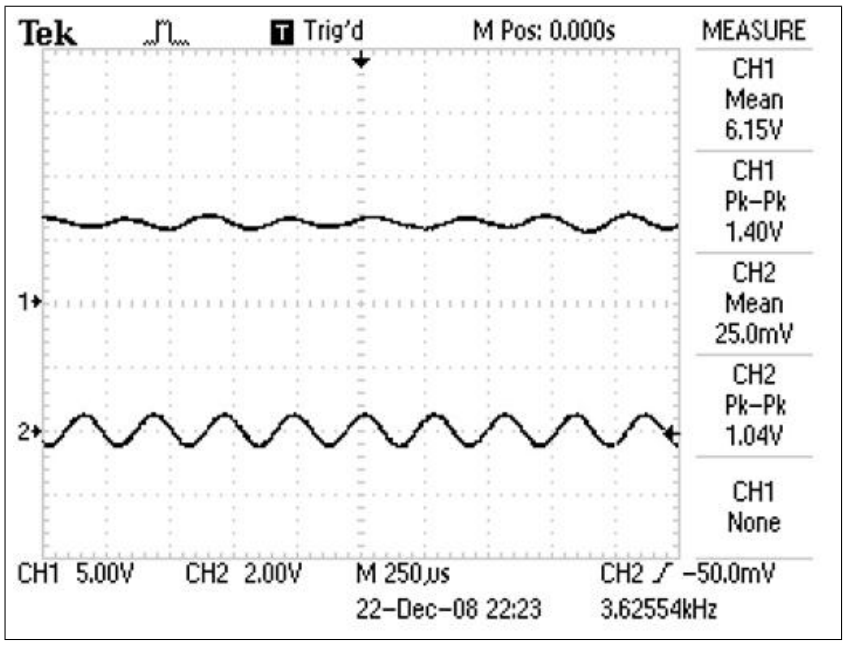

Figure 4.19 For 3.625 KHz input, the response of the second filter (pass-band: 2700-3300, channel 2 input, channel 1 output)

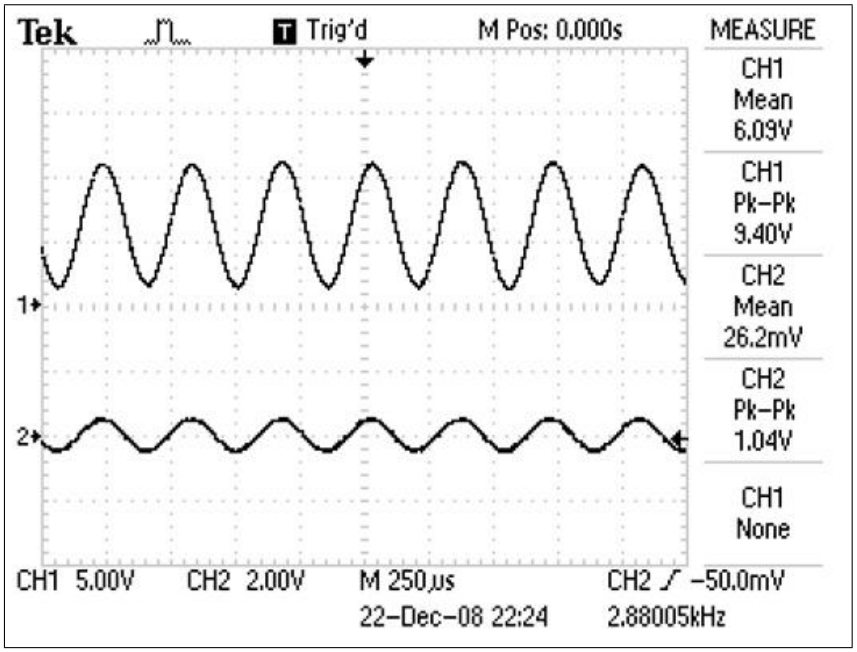

Figure 4.20 For 2.888 KHz input, the response of the second filter (pass-band: 2700-3300, channel 2 input, channel 1 output)

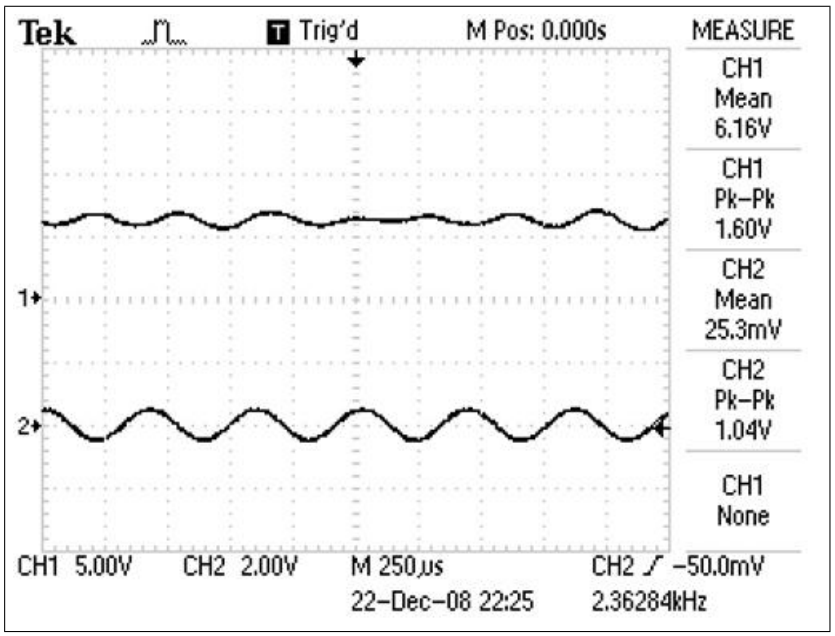

Figure 4.21 For 2.362 KHz input, the response of the second filter (pass-band: 2700-3300, channel 2 input, channel 1 output)

4.2.5 Peak Detector

The transmitted light after passing the filters will carry with the frequency the led driven, the response of the tissue of interest. To detect the response of the tissue the signal must be passed from a peak detector. This crucial for the system because that is what we are looking for.

For peak detection the circuit in the figure 4.22 is used. The operational amplifier used is LM324, and diode is 1N4007 general purpose rectifier. The potentiometer is used for gain adjustments.

4.2.6 DAQ and PC

For data acquisition Labview program and a DAQ card both supplied from the Boğaziçi University is used. The program prepared with Labview 6.0 is shown in figure 4.24. This program is used for 4 channels from the two detectors.

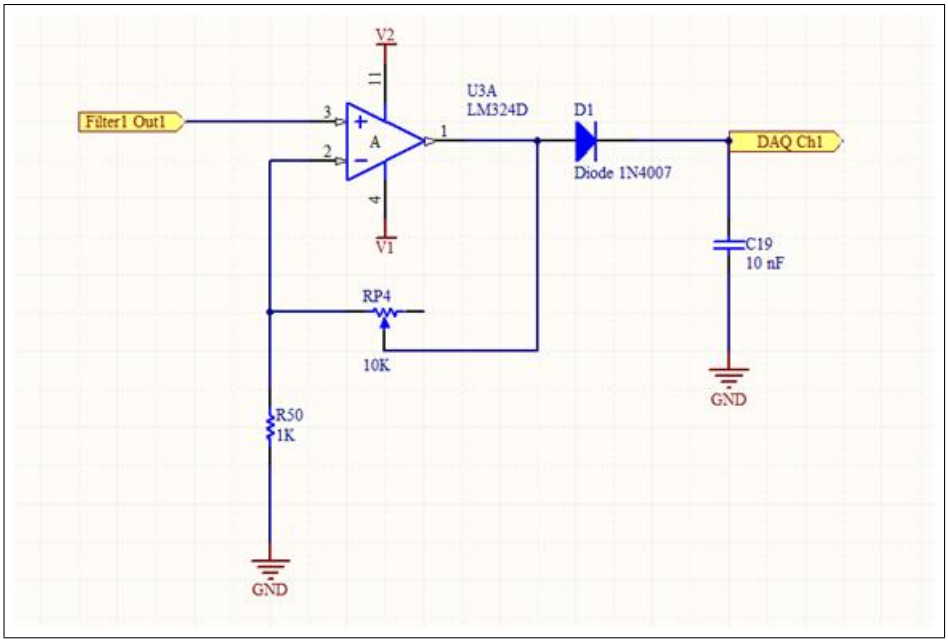

Figure 4.22 The peak detector used for channel 1.

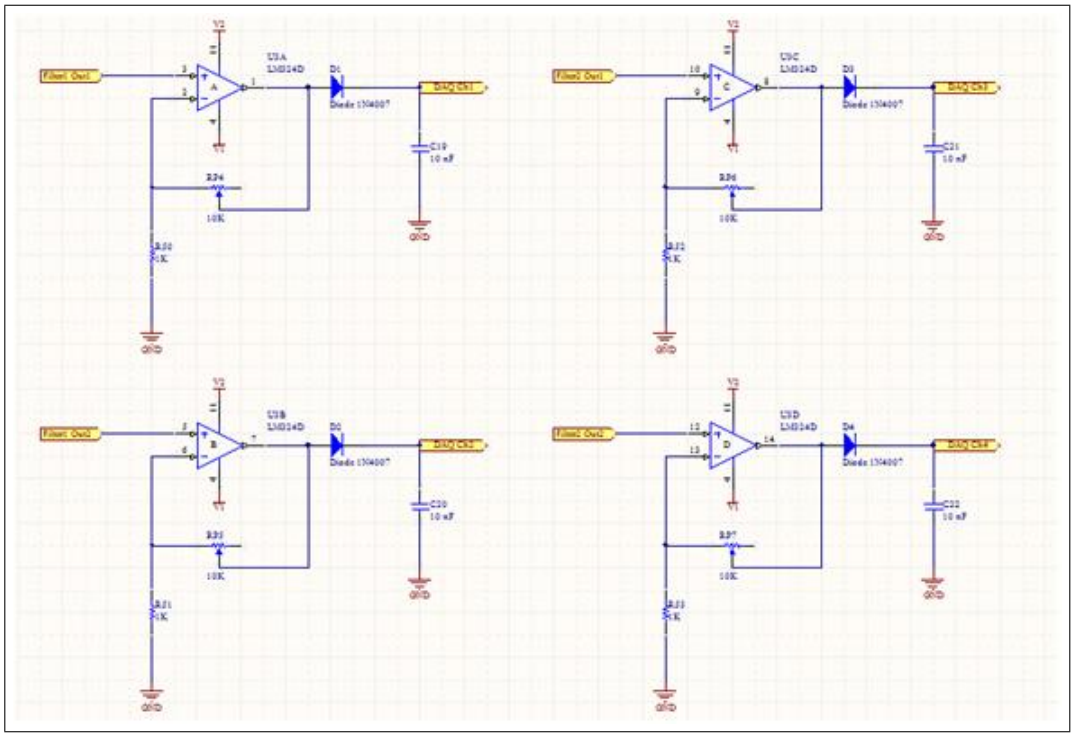

Figure 4.23 The peak detectors for the four channels.

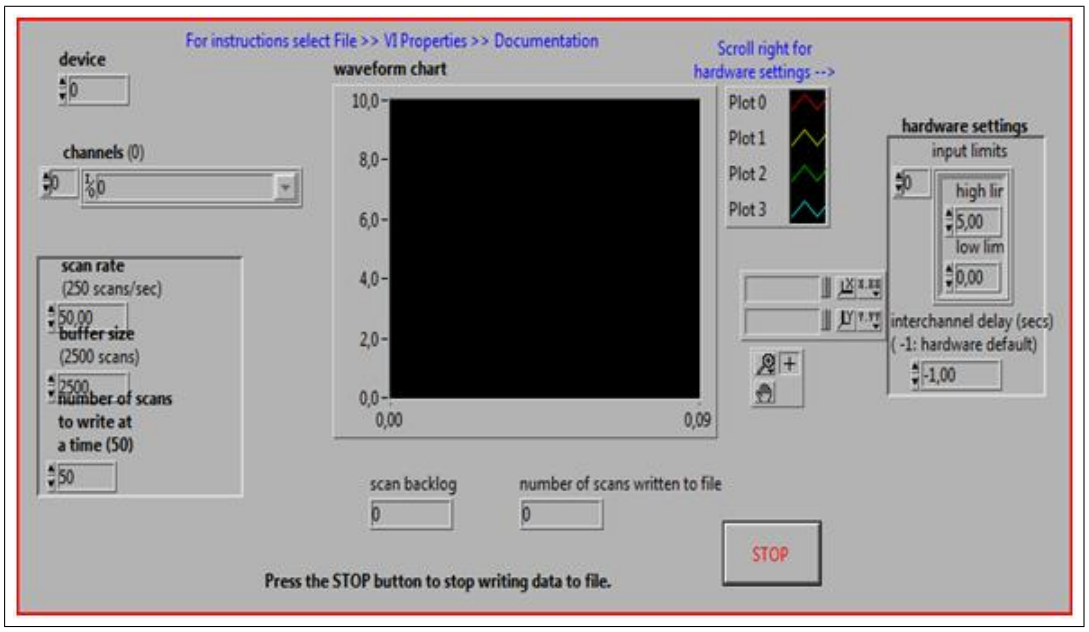

Figure 4.24 The LabView program used to continuously collect data and write to a spread-sheet.

National Instrument NI PCI-MIO-16E-4 card is the DAQ card used for data acquisition. This card provides up to 250 kS/s multi-channel sampling rate.

4.3 The Instrument

The box of the device has the dimensions $25cm \cdot 23cm \cdot 8cm(L \cdot W \cdot H)$, and black as its color. For cooling purposes box is chosen with holes on the upper side of the box. Also the system uses a low noise fan and metal coolers for regulators.

The probe is mainly designed for the use on the arm. But it can also be used in the in the head. A cooler is added to probe design so that the overheating during the operation will be eliminated.

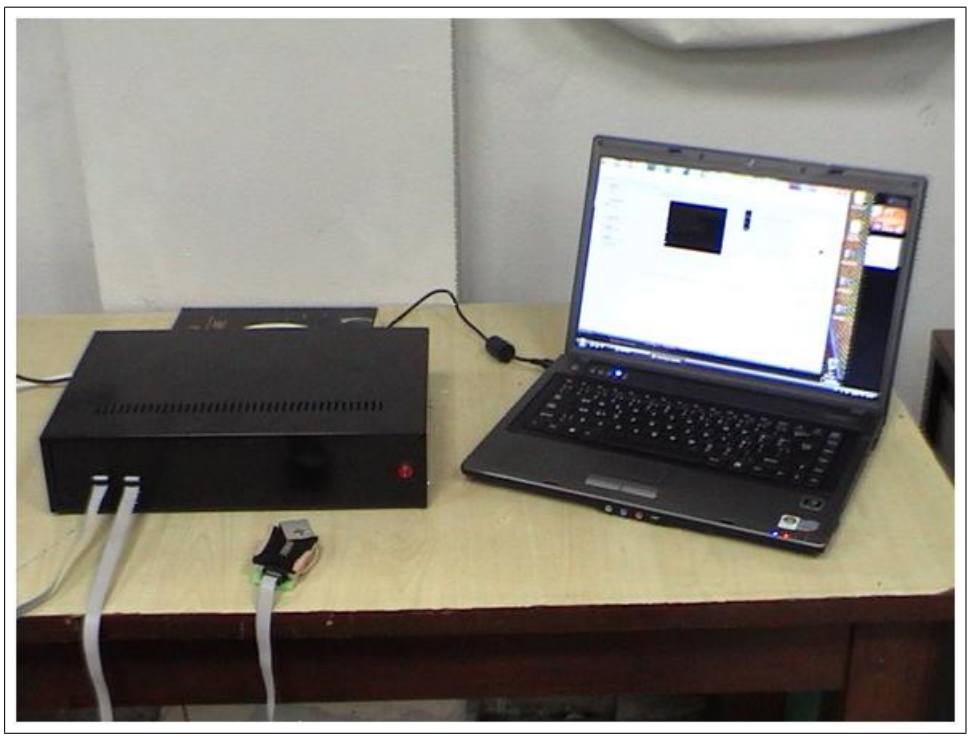

Figure 4.25 The device that was built (right), the probe (bottom left)

Figure 4.26 The probe used for measurements, (A) the led, (B) The detectors (C) the cooler.

4.4 The Results

The instrument, after being tested on phantoms, is used in experiments and measurements are recorded from humans. Two kinds of measurements around 5 minutes are taken from subjects. First for the ischemia condition measurements are taken from right arm, and second for breath holding measurements are taken from the head. The analysis of the data gathered from the experiment are done by using Beer - Lambert Law in Matlab version 7.0.

- Ischemia
- Breath holding

4.4.1 Protocols

Two different protocols are used for ischemia and breathe holding measurements since the measurements are taken from different part of the body with different functions.

4.4.1.1 Ischemia Protocol. For measurements from the lower arm ischemia is chosen. The procedure is as follows:

- For 3-4 minutes measurements are made from the right arm at rest.
- The probe is fixed over muscle tissue of the lower right or left arm
- Measurements for 1 minute is taken at rest
- Then the blood supply is cut with the artificial ischemia applied with a inflatable air-bladder cuff of an standard sphygmomanometer
- Then recordings are taken for 1 minute for ischemia condition

- At last, the pressure applied with cuff is cut
- Measurement at rest for a minute is taken

4.4.1.2 Breath Holding. For the measurements taken from the head, breath holding procedure is chosen. The procedure is as follows:

- For 4-5 minutes measurements are made for the forehead.
- The probe is fixed over forehead tissue
- Measurements for 1 minute is taken
- Then subject starts to hold his/her breath
- Recordings are taken for 45 seconds
- Then the subject starts to breath
- Measurements for 1 minute is taken at rest
- Then subject starts to hold his/her breath again
- Recordings for a minute is taken
- Then subject starts to breathe again
- Measurement for a minute is taken

4.4.2 Results of Ischemia Procedure

The artificial ischemia that is created by the air-bladder cuff of an standard sphygmomanometer stops the transport of the blood to the arm for a period of time. During this time arm is not supplied with blood. So the blood inside the arm has a limited amount of oxygen supply. With time, the tissues in the arm use the oxygen

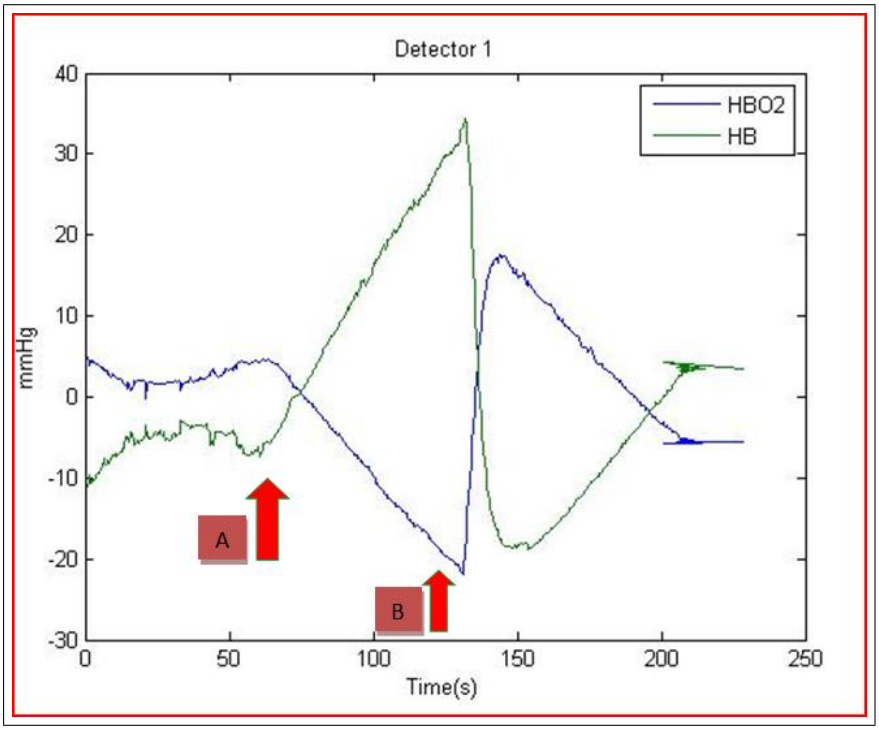

Figure 4.27 The oxy-Hb and Deoy-Hb concentrations (lower arm measurement) calculated with the modified Beer-Lambert Law from the detector that is at 2 cm on the probe.

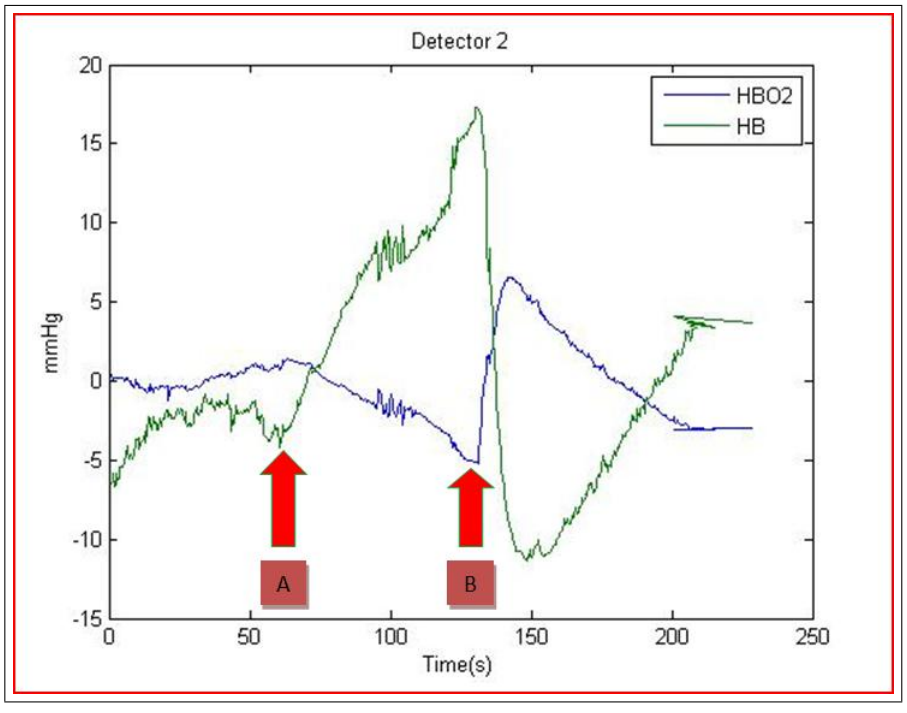

Figure 4.28 The oxy-Hb and Deoy-Hb concentrations (lower arm measurement) calculated with the modified Beer-Lambert Law from the detector that is at 3 cm on the probe.

in the blood. Since the transport of oxygenated blood is cut, it is expected that the amount of oxy-Hb decreases with time and the deoxy-Hb concentration increases with time. The results of the experiment provide evidence in that direction as seen from the figures 4.27, and 4.28.

The figure 4.27 and 4.28 clearly shows that around 1 minute (A) the oxy-Hb concentration start to decrease and the deoxy-Hb concentration starts to increase with the start of ischemia. Figure 4.27 and 4.28 also shows that around two minutes (B) the oxy-Hb concentration start to increase and the deoxy-Hb concentration starts to decrease with the end of ischemia.

4.4.3 Results of Breath Holding Procedure

To see the concentration change in the blood haemoglobin, breath holding is used. During breath holding the oxygen supply of the body is consumed quickly and since the breath is held, the oxygen supply of the body can not be renewed. So the brain has a limited amount of oxygen supply. With time, the brain uses the oxygen that is available in the blood. Since the transport of oxygenated blood is temporally stopped, it is expected that the amount of oxy-Hb decreases with time and the deoxy-Hb concentration increases with time. The results of the experiment provide evidence in that direction as seen from the figures 4.29, and 4.30.

The figure 4.29 and 4.30 clearly shows that around 1 minute (A) the oxy-Hb concentration start to decrease and the deoxy-Hb concentration starts to increase with the start of first breath hold and around 90 seconds (B) the oxy-Hb concentration start to increase and the deoxy-Hb concentration starts to decrease with the end of first breath hold. Around 120 seconds (C) the oxy-Hb concentration start to decrease and the deoxy-Hb concentration starts to increase with the start of second breath hold and around 180 seconds (D) the oxy-Hb concentration start to increase and the deoxy-Hb concentration starts to decrease with the end of second breath hold.

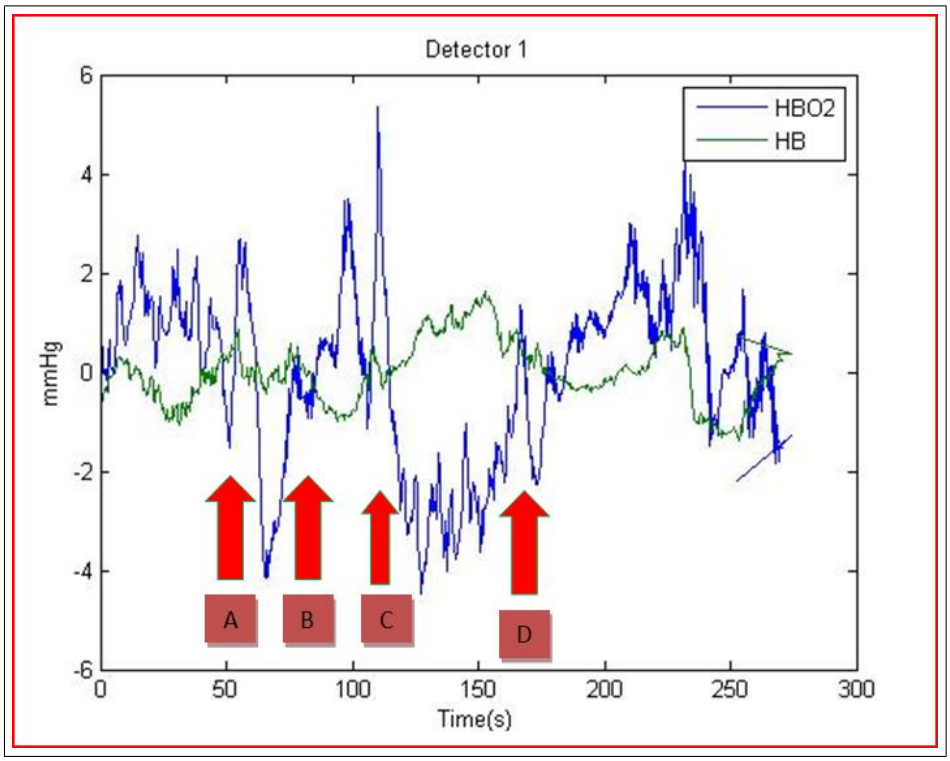

Figure 4.29 The oxy-Hb and Deoy-Hb concentrations (forehead measurement) calculated with the modified Beer-Lambert Law from the detector that is at 2 cm on the probe.

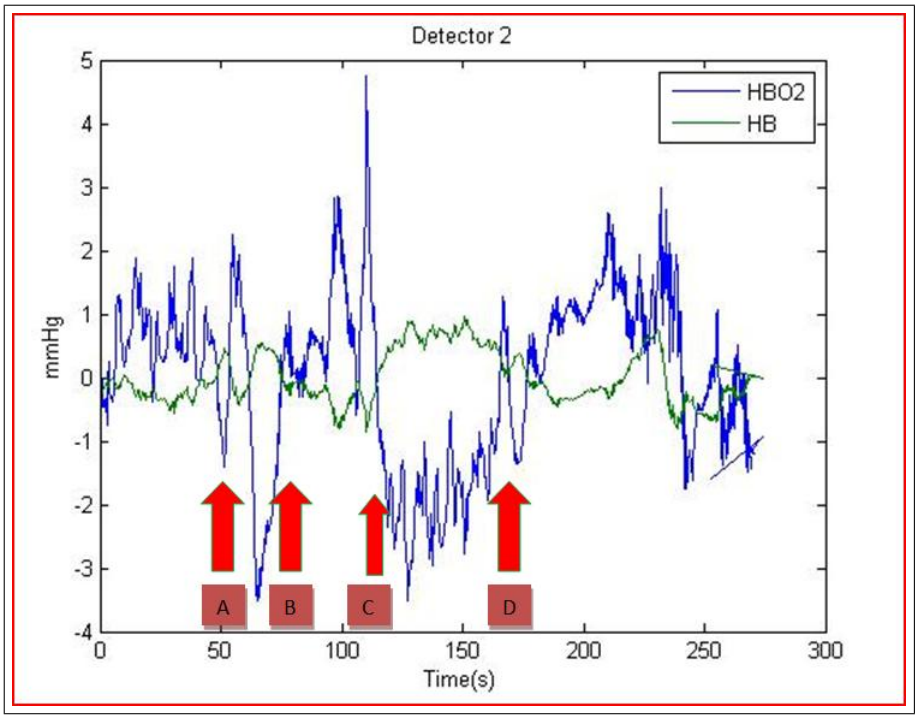

Figure 4.30 The oxy-Hb and Deoy-Hb concentrations (forehead measurement) calculated with the modified Beer-Lambert Law from the detector that is at 3 cm on the probe.

5. Conclusions and Future Work

5.1 Summary

In this study a continuous wave near-infrared spectroscopy instrument is developed. The instrument is used to measure successfully both of the wavelengths at the same time. The system has four channels that provide the output from two detectors.

5.2 Discussion

The instrument designed has proven its reliability on human subjects. The expected decrease and increases in the Hb and HbO2 concentrations are seen in the measurements. This system is faster and more reliable than the previous version, NIROOXCOPE. The sample rate is increased to 50 Hz. The signal to noise ratio and electromagnetic interference is decreased. This system by not using the multiplexer, simplified the circuitry.

5.3 Future Work

It is seen that the instrument is affected by the strong electromagnetic sources like cell phones that are around it. Also motion artifacts cause measurements errors due to the intensity change in the transmitted light. The probe design is suitable for head measurements but limits the area of interest because of its design.

Future work should be focused on improving the performance of the system. The SNR ratio and the electromagnetic interference should be decreased by optimizing and improving the PCB design, shielding the cables or using shielded cables. Also the probe design should be modified to be better suited on the human head.

APPENDIX A. INDIVIDUAL MEASUREMENTS

A.1 Ischemia Results

A.1.1 Subject 1

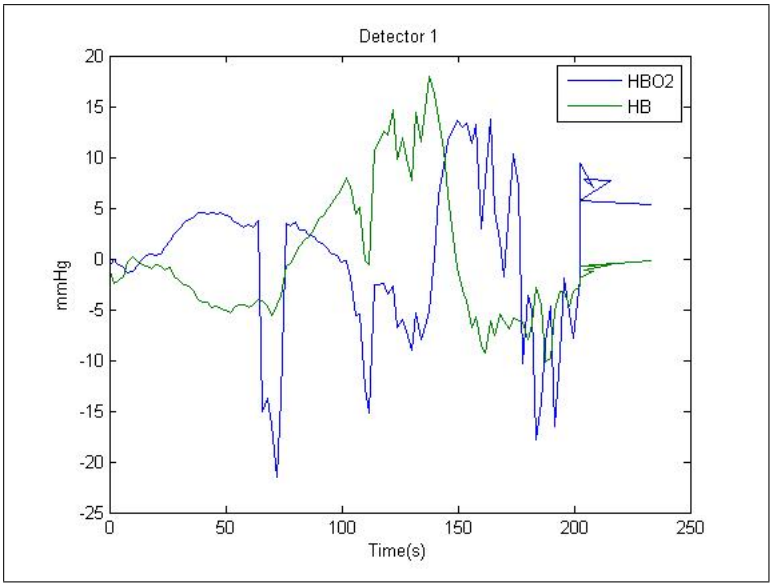

Figure A.1 The oxy-Hb and Deoy-Hb concentrations (lower arm measurement) calculated with the modified Beer-Lambert Law from the detector that is at 2 cm on the probe.

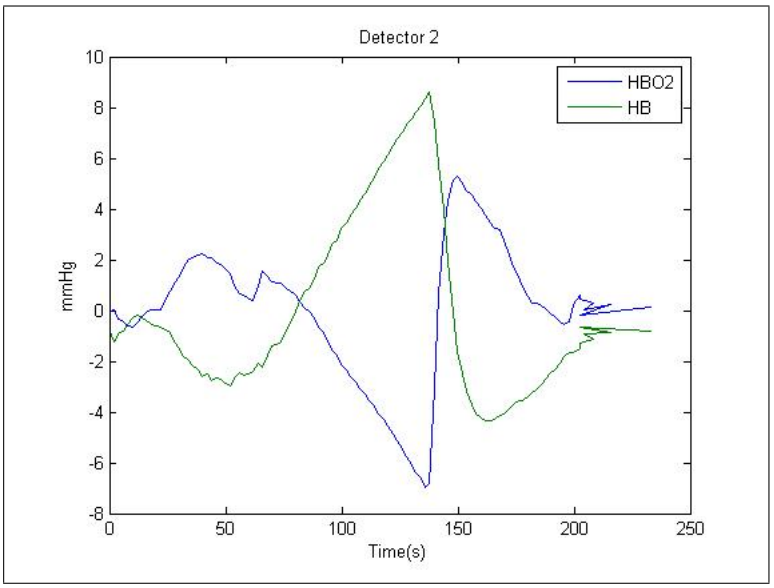

Figure A.2 The oxy-Hb and Deoy-Hb concentrations (lower arm measurement) calculated with the modified Beer-Lambert Law from the detector that is at 3 cm on the probe.

A.1.2 Subject 2

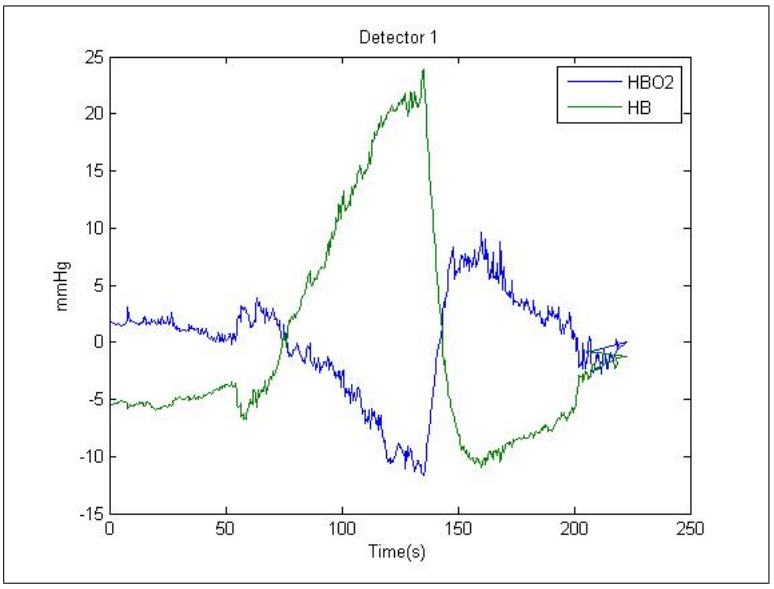

Figure A.3 The oxy-Hb and Deoy-Hb concentrations (lower arm measurement) calculated with the modified Beer-Lambert Law from the detector that is at 2 cm on the probe.

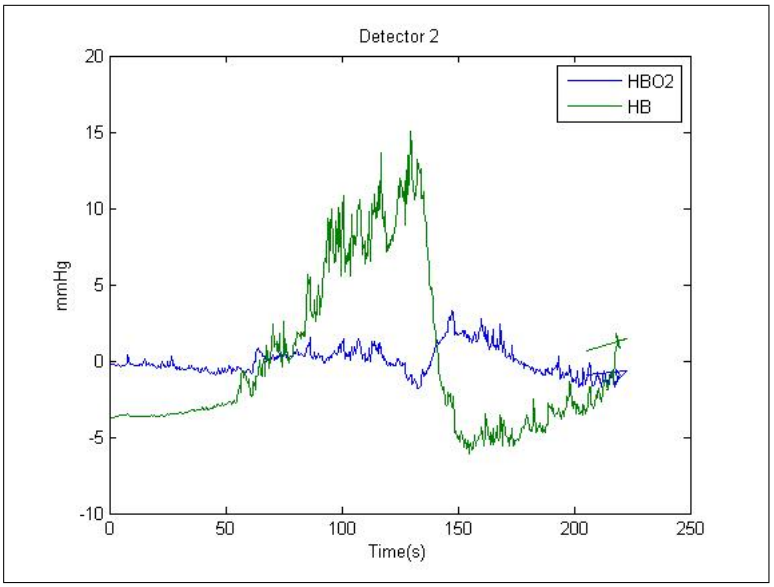

Figure A.4 The oxy-Hb and Deoy-Hb concentrations (lower arm measurement) calculated with the modified Beer-Lambert Law from the detector that is at 3 cm on the probe.

A.1.3 Subject 3

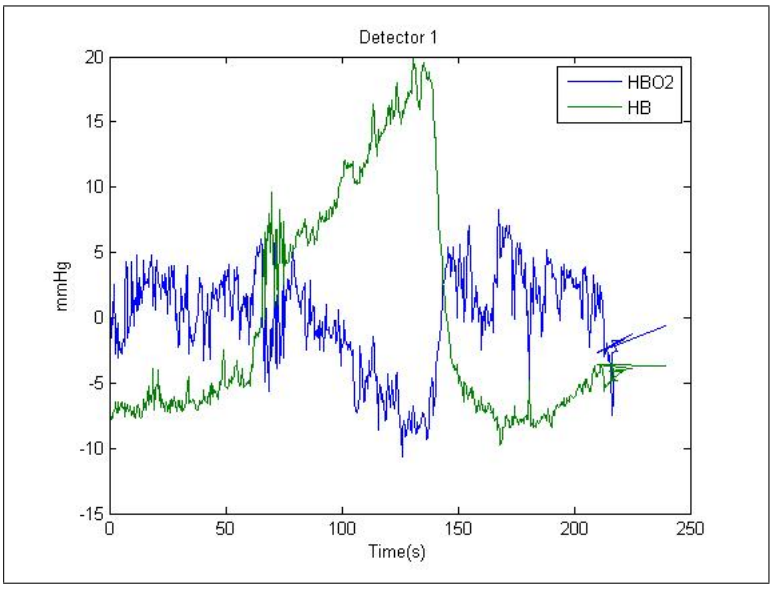

Figure A.5 The oxy-Hb and Deoy-Hb concentrations (lower arm measurement) calculated with the modified Beer-Lambert Law from the detector that is at 2 cm on the probe.

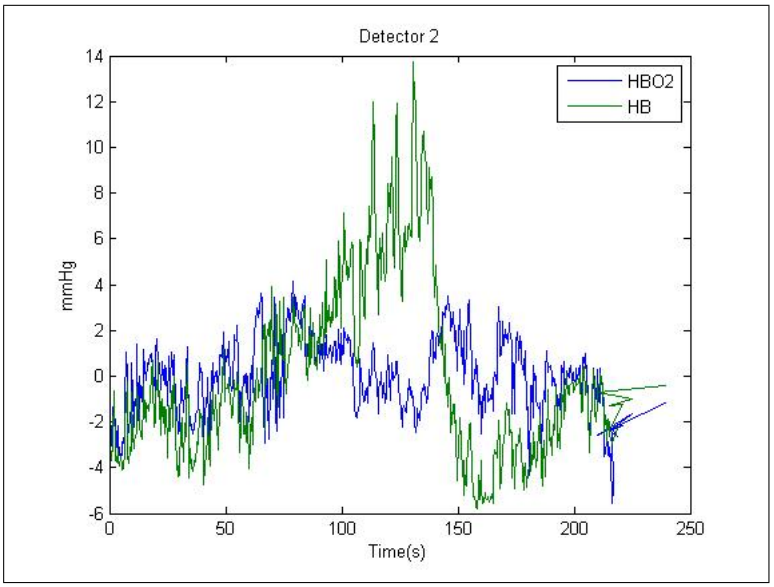

Figure A.6 The oxy-Hb and Deoy-Hb concentrations (lower arm measurement) calculated with the modified Beer-Lambert Law from the detector that is at 3 cm on the probe.

A.1.4 Subject 4

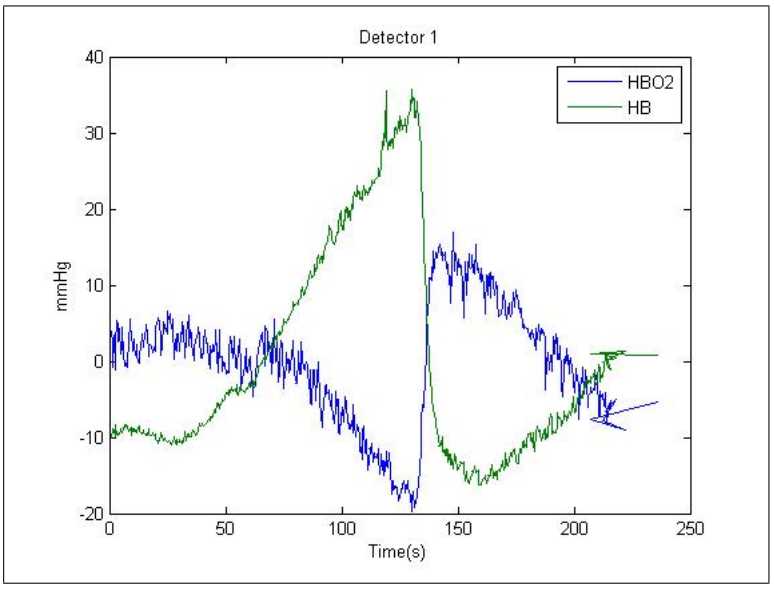

Figure A.7 The oxy-Hb and Deoy-Hb concentrations (lower arm measurement) calculated with the modified Beer-Lambert Law from the detector that is at 2 cm on the probe.

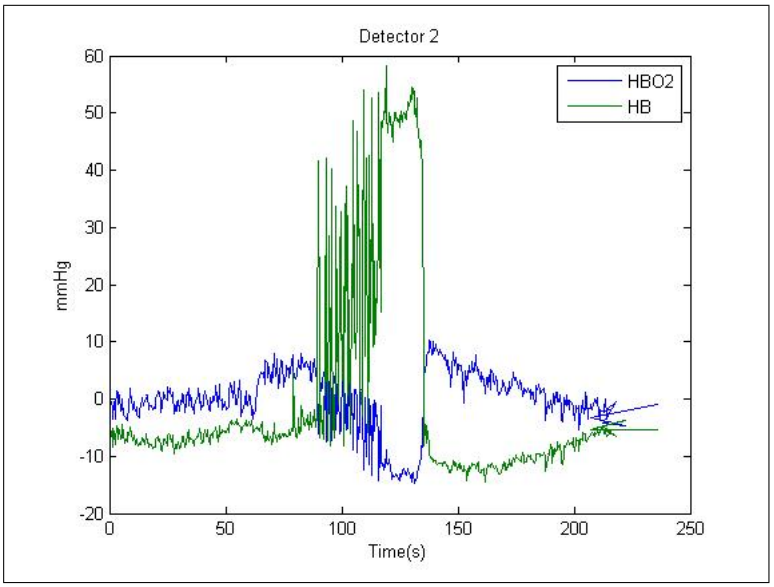

Figure A.8 The oxy-Hb and Deoy-Hb concentrations (lower arm measurement) calculated with the modified Beer-Lambert Law from the detector that is at 3 cm on the probe.

A.1.5 Subject 5

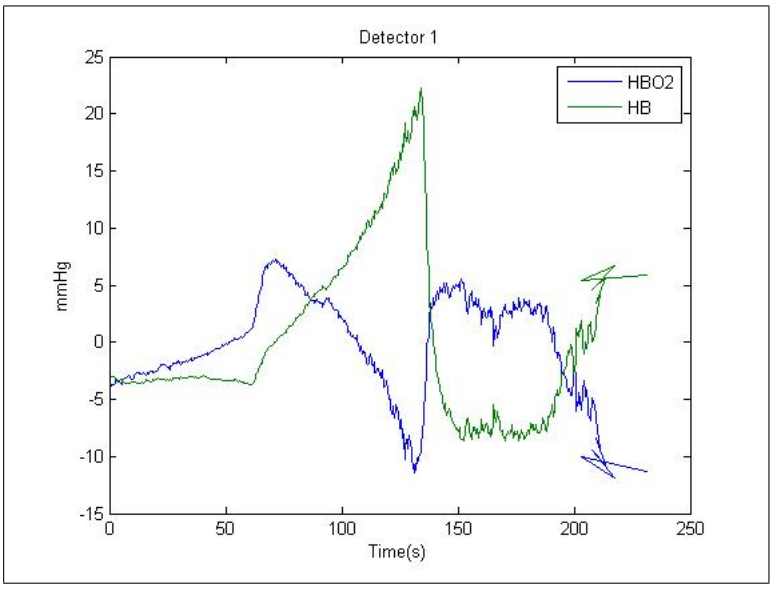

Figure A.9 The oxy-Hb and Deoy-Hb concentrations (lower arm measurement) calculated with the modified Beer-Lambert Law from the detector that is at 2 cm on the probe.

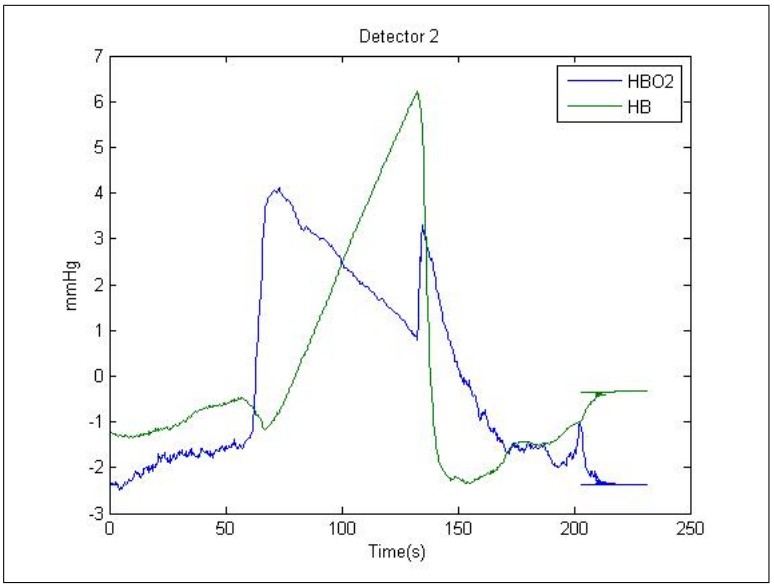

Figure A.10 The oxy-Hb and Deoy-Hb concentrations (lower arm measurement) calculated with the modified Beer-Lambert Law from the detector that is at 3 cm on the probe.

A.1.6 Subject 6

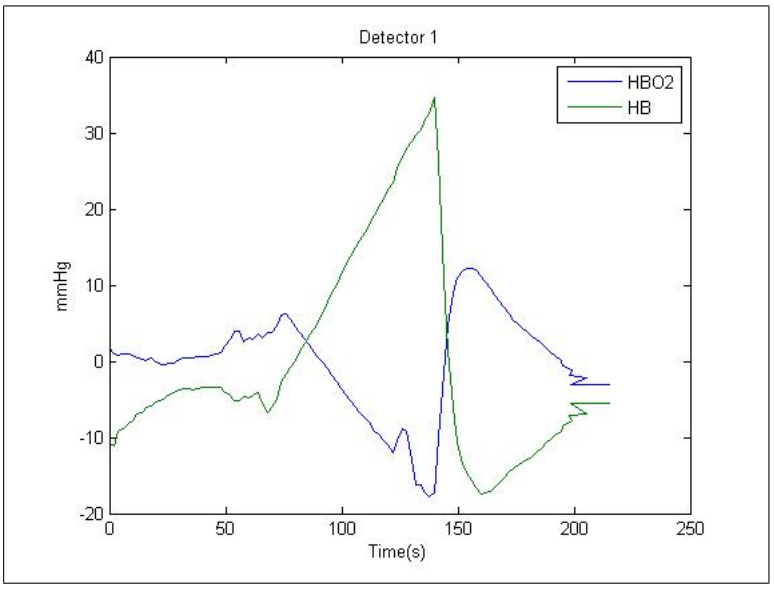

Figure A.11 The oxy-Hb and Deoy-Hb concentrations (lower arm measurement) calculated with the modified Beer-Lambert Law from the detector that is at 2 cm on the probe.

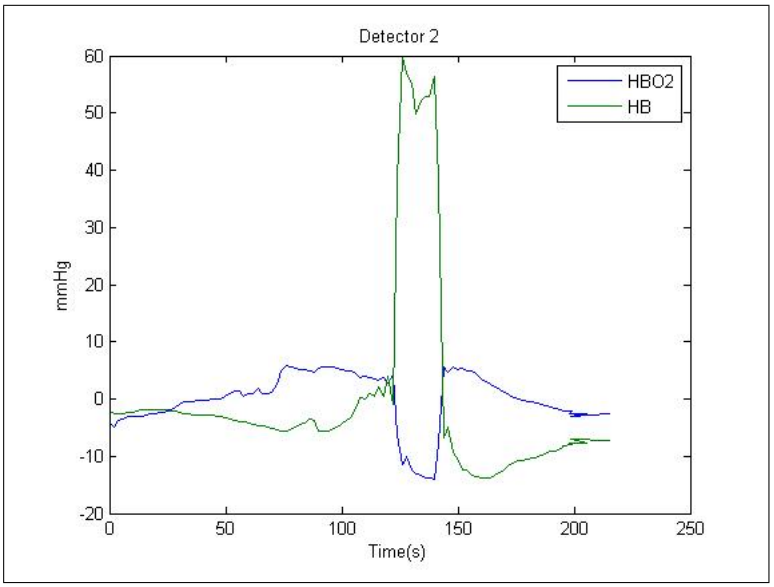

Figure A.12 The oxy-Hb and Deoy-Hb concentrations (lower arm measurement) calculated with the modified Beer-Lambert Law from the detector that is at 3 cm on the probe.

A.2 Breath Holding Results

A.2.1 Subject 1

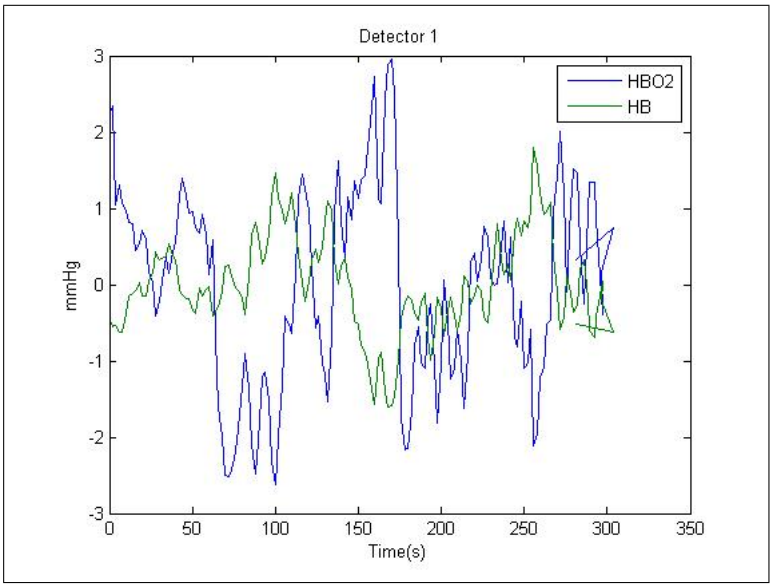

Figure A.13 The oxy-Hb and Deoy-Hb concentrations (forehead measurement) calculated with the modified Beer-Lambert Law from the detector that is at 2 cm on the probe.

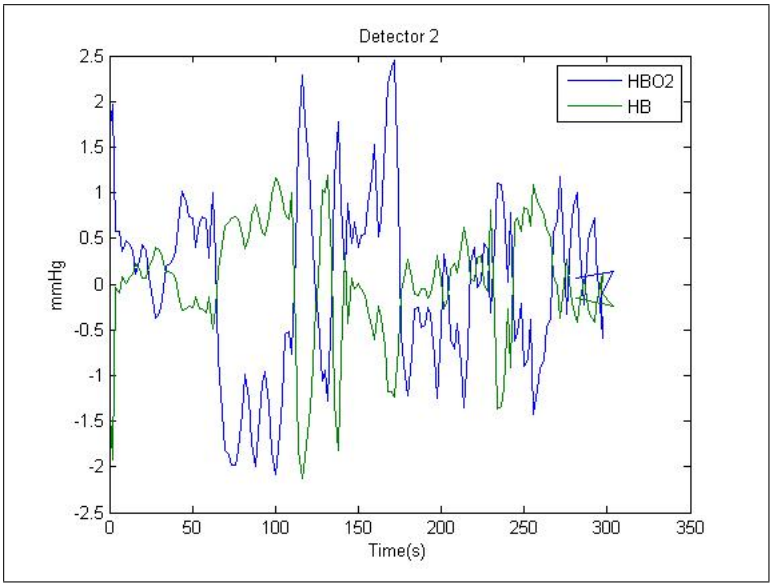

Figure A.14 The oxy-Hb and Deoy-Hb concentrations (forehead measurement) calculated with the modified Beer-Lambert Law from the detector that is at 3 cm on the probe.

A.2.2 Subject 2

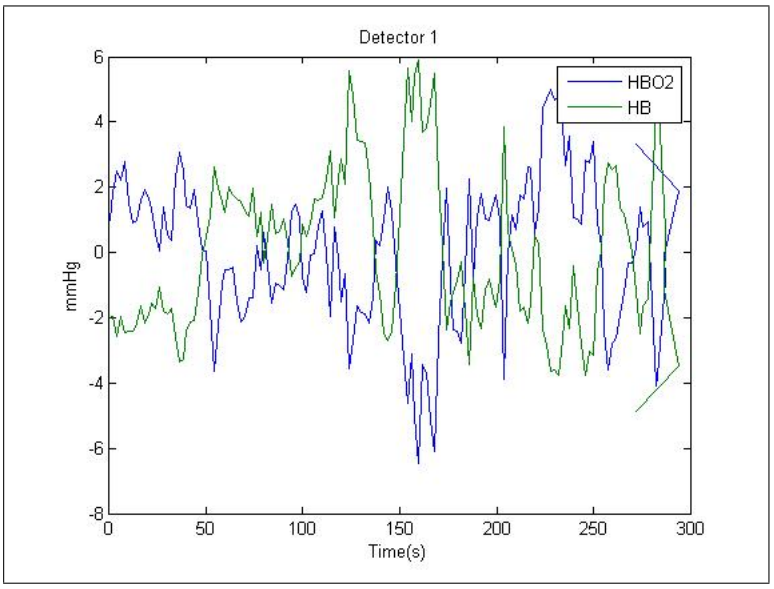

Figure A.15 The oxy-Hb and Deoy-Hb concentrations (forehead measurement) calculated with the modified Beer-Lambert Law from the detector that is at 2 cm on the probe.

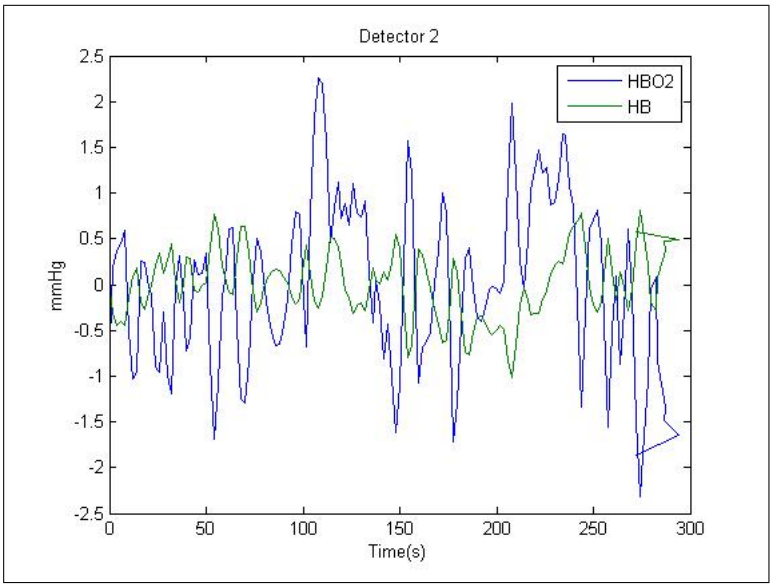

Figure A.16 The oxy-Hb and Deoy-Hb concentrations (forehead measurement) calculated with the modified Beer-Lambert Law from the detector that is at 3 cm on the probe.

A.2.3 Subject 3

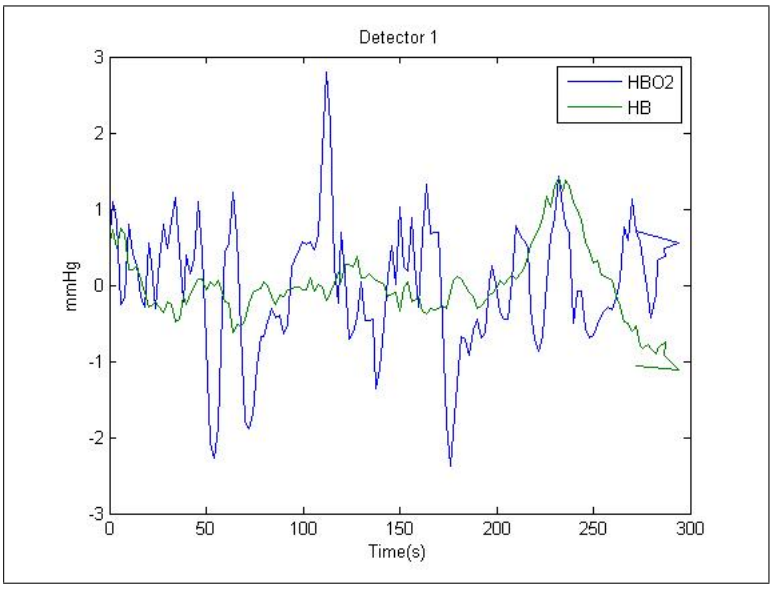

Figure A.17 The oxy-Hb and Deoy-Hb concentrations (forehead measurement) calculated with the modified Beer-Lambert Law from the detector that is at 2 cm on the probe.

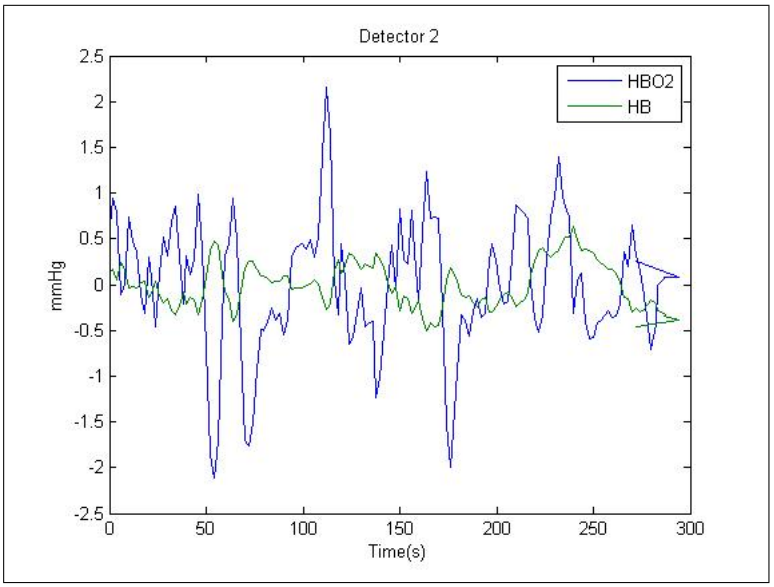

Figure A.18 The oxy-Hb and Deoy-Hb concentrations (forehead measurement) calculated with the modified Beer-Lambert Law from the detector that is at 3 cm on the probe.

A.2.4 Subject 4

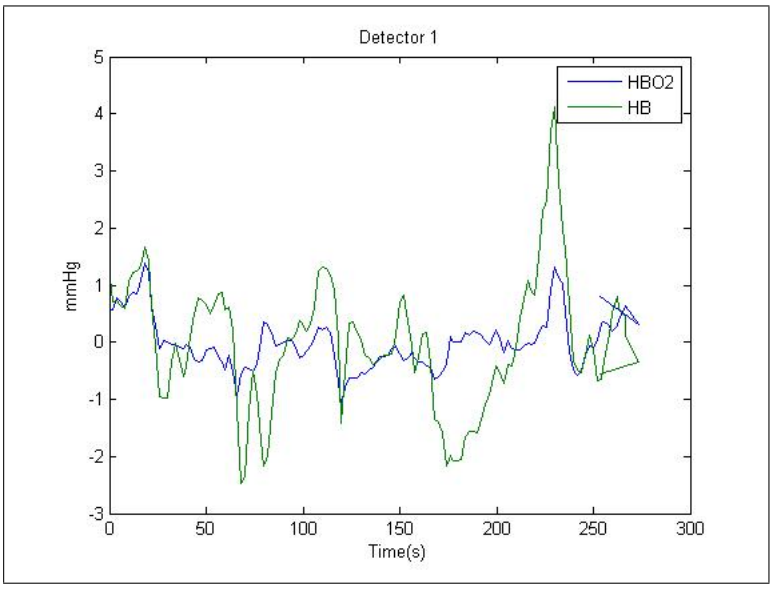

Figure A.19 The oxy-Hb and Deoy-Hb concentrations (forehead measurement) calculated with the modified Beer-Lambert Law from the detector that is at 2 cm on the probe.

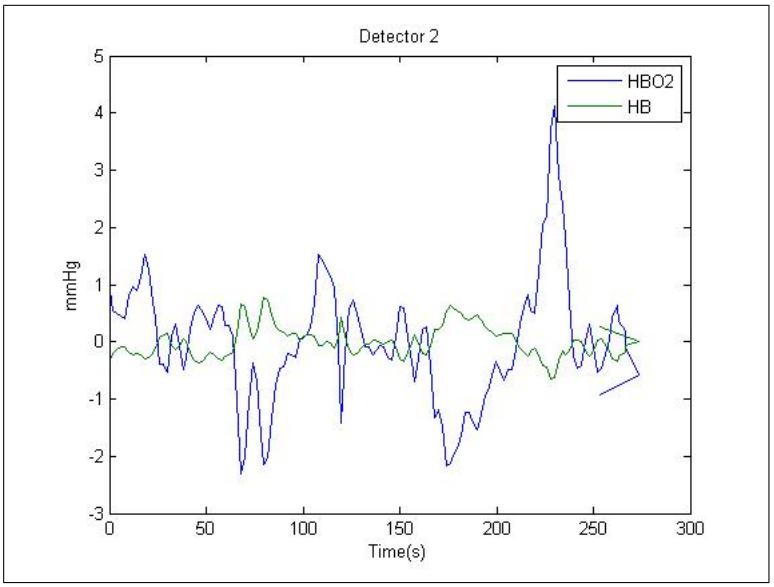

Figure A.20 The oxy-Hb and Deoy-Hb concentrations (forehead measurement) calculated with the modified Beer-Lambert Law from the detector that is at 3 cm on the probe.

A.2.5 Subject 5

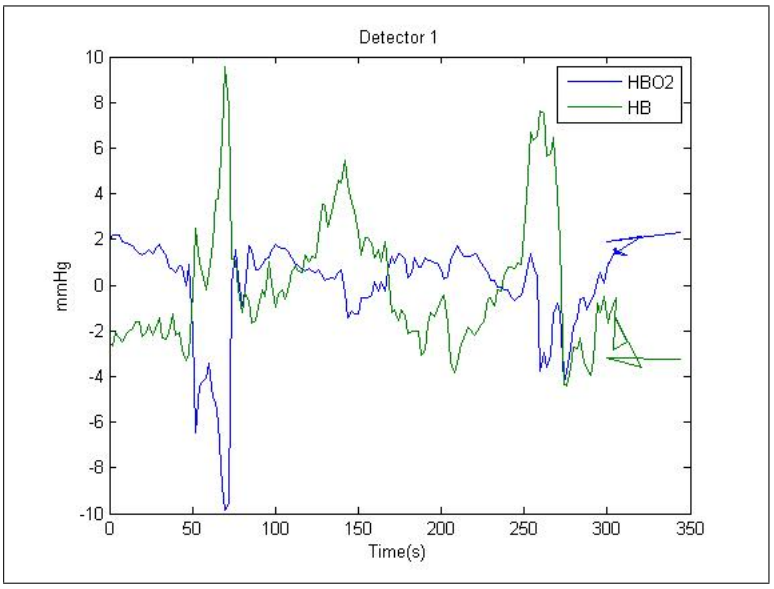

Figure A.21 The oxy-Hb and Deoy-Hb concentrations (forehead measurement) calculated with the modified Beer-Lambert Law from the detector that is at 2 cm on the probe.

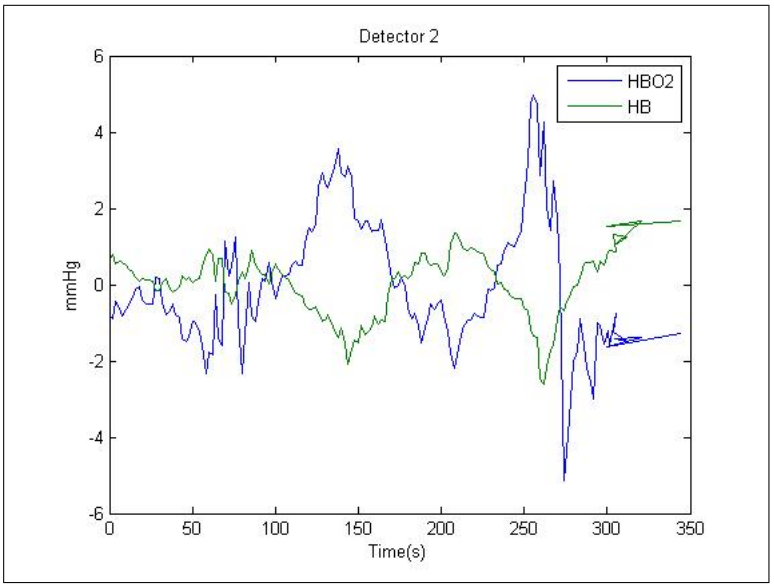

Figure A.22 The oxy-Hb and Deoy-Hb concentrations (forehead measurement) calculated with the modified Beer-Lambert Law from the detector that is at 3 cm on the probe.

REFERENCES

1. "Wikipedia." http://en.wikipedia.org/wiki/File:EM_Spectrum_Properties_edit.svg.
2. "ISS." http://http://www.iss.com/products/imagent/about.html.
3. Gray, H., *Henry Gray's Anatomy of the Human Body*, 1980.
4. "Lesson materials of BME586 - SKELETAL MUSCLE MECHANICS."
5. Emir, U. E., *System Charcterization for a Fast Optical Imager*. PhD thesis, Boğaziçi University, İstanbul, Turkey, 2003.
6. "UCL Department Of Medical Physics And Bioengineering Faculty Of Engineering Sciences,Biomedical Optic Research Laboratory." http://www.medphys.ucl.ac.uk/research/borl/research/NIR_topics/nirs.htm.
7. Schmidt, F. E. W., *Development of a Time-Resolved Optical Tomography System for Neonatal Brain Imaging*. PhD thesis, University of London, London, England, 1999.
8. Yu, G., T. Durduran, G. Lech, C. Zhou, B. Chance, E. R. Mohler, and A. G. Yodh, "Time-dependent blood flow and oxygenation in human skeletal muscles measured with noninvasive near-infrared diffuse optical spectroscopies," *Journal of biomedical Optics*, March/April 2005.
9. "Stem type led l4*730/4*805/4*850-40q96-i," *Datasheet, Epitex*.
10. "OPT101 monolithic photodiode and single-supply transimpedance amplifier," *Datasheet, Texas Instruments*.
11. Wolf, M., M. Ferrari, and V. Quaresima, "Progress of near-İnfrared spectroscopy and topography for brain and muscle clinical applications," *Journal of Biomedical Optics*, Vol. 12, November/December 2007.
12. Yang, Y., O. O. Soyemi1, P. J. Scott, M. R. Landry, S. M. C. L. andL. Stroud, and B. R. Soller, "Quantitative measurement of muscle oxygen saturation without influence from skin and fat using continuous-wave near infrared spectroscopy," *Optics Express*, Vol. 15, October 2007.
13. Bunce, S. C., M. İzzetoğlu, K. İzzetoğlu, B. Onaral, and K. Pourrezaei, "Functional near-infrared spectroscopy: An emerging neuroimaging modality," *IEEE Engineering In Medicine And Biology Magazıne*, July/August 2006.
14. Obrig, H., and A. Villringer, "Beyond the visible-imaging the human brain with light," 2003.
15. Boushel, R., and C. A. Piantadosi, "Near-infrared spectroscopy for monitoring muscle oxygenation," *Scandinavian Physiological Society*, 2000.
16. Coyle, S. M., T. E. Ward, and C. M. Markham, "Brain-computer interface using a simplified functional near-infrared spectroscopy system," *Journal of Neural Engineering*, pp. 219–226, 2007.
17. Matthews, F., B. A. Pearlmutter, T. E. Ward, C. Soraghan, and C. Markham, "Hemodynamics for brain-computer interfaces: Optical correlates of control signals," *IEEE Signal Processing Magazine*, pp. 87–94, January 2008.

18. Burns, D. A., and E. W. Ciurczak, *Handbook of Near-Infrared Analysis, 3rd ed.*, CRC Press, 2008.

19. Zee, P. V. D., *Measurement and Modeling of the Optical Properties of Human Tissue in the Near Infrared.* PhD thesis, University Of London, London, England, 1992.

20. "ICL8038, precision waveform generator/voltage controlled oscillator," *Datasheet, Intersil.*

21. Scherz, P., *Practical Electronics for Inventers*, McGraw Hill, 2006.

22. Sedra, A. S., and K. C. Smith, *Microelectronic Circuits, Oxford University Press, 5th ed.*, Oxford University Press, 2004.